Gutzwiller electronic structure calculations applied to transition metals: Kinetic energy gain with ferromagnetic order in bcc Fe

Giovanni Borghi,[1,2,*] Michele Fabrizio,[2,†] and Erio Tosatti[2,3,4,‡]

[1]*Theory and Simulation of Materials, École Polytechnique Fédérale de Lausanne EPFL, CH-1015 Lausanne, Switzerland*

[2]*International School for advanced studies (SISSA), via Bonomea 265, 34136 Trieste, Italy*

[3]*CNR-IOM Democritos, via Bonomea 265, 34136 Trieste, Italy*

[4]*The Abdus Salam International Centre for Theoretical Physics (ICTP), Strada Costiera 11, 34151 Trieste, Italy*

(Received 8 June 2014; revised manuscript received 4 August 2014; published 2 September 2014)

The Gutzwiller projector technique has long been known as a method to include correlations in electronic structure calculations. We describe a model implementation for a Gutzwiller + LDA calculation in a localized-orbital restricted basis framework, emphasizing the protocol step by step and illustrating our specific procedure for this and future applications. We demonstrate the method with a classic problem, the ferromagnetism of bulk bcc Fe, whose nature is attracting fresh interest. In the conventional Stoner-Wohlfarth model, and in spin-polarized LDA calculations, the ferromagnetic ordering of iron sets in so that the electrons can reduce their mutual Coulomb repulsion, at the cost of some increase of electron kinetic energy. This balance may, however, be altered by correlations, which are strong for localized d orbitals. The present localized basis Gutzwiller + LDA calculation demonstrates how the ferromagnetic ordering of Fe may, in fact, entrain a decrease of kinetic energy at the cost of some increase of potential energy. This happens because, as foreshadowed long ago by Goodenough and others and more recently supported by LDA-DMFT calculations, correlations cause e_g and t_{2g} d orbitals to behave differently, with the weakly propagating e_g states fully spin polarized and almost localized, and only t_{2g} states forming a broad partly filled itinerant band. Owing to an intra-atomic Hund's rule exchange that aligns e_g and t_{2g} spins, the propagation of itinerant t_{2g} holes is favored when different atomic spins are ferromagnetically aligned. This suggests a strong analogy with double exchange in iron ferromagnetism.

DOI: 10.1103/PhysRevB.90.125102 PACS number(s): 71.15.−m, 71.30.+h, 71.20.Be, 75.50.Bb

I. INTRODUCTION

The conduction d electron Wannier orbitals in transition-metal compounds are generally fairly localized in space so that electronic correlations, i.e., all effects that deviate from the independent-particle picture, are sometimes strong enough to give rise to metal-insulator transitions in certain temperature and pressure conditions. The correlation-driven metal-insulator transition, known as Mott transition [1,2], is often accompanied by rather spectacular phenomena that appear in its proximity, high-temperature superconductivity in cuprates, and colossal magnetoresistance in manganites being popular examples. This makes $3d$ metal elements and compounds a natural laboratory for many-body physics, which, despite a rich history and many studies, may still hold surprises.

First-principles electronic structure calculations that build upon independent-particle descriptions, such as Hartree-Fock (HF) or density functional theory (DFT) within local density approximation (LDA), while constituting the bread-and-butter basis for most quantitative solid-state physics and generally quite successful for elemental transition metals, may be exposed to failure in the description of the properties of compounds involving transition metals and stronger correlations. These systems are usually treated by model-based techniques such as quantum Monte Carlo [3], density-matrix renormalization group [4], and dynamical mean-field theory [5]. Clearly, for the purpose of the overall understanding of real materials, it is of key importance to sew the two worlds together, bringing in particular the many-body expertise gained on lattice models over to realistic, off-lattice, first-principles calculations of solids. In the context of lattice models, a simple approach to strong correlations was proposed long ago by Gutzwiller [6,7]. This method, projecting out of a trial Slater determinant an adjustable proportion of energetically costly configurations and evaluating average values by approximate formulas, is strictly variational in the limit of infinite lattice coordination [8]—the same limit where dynamical mean-field theory (DMFT) is exact—providing much more accurate results than HF. That success invites the use of the Gutzwiller method even when the lattice space dimension, and thus the site coordination, is finite, as people do with DMFT. Unlike DMFT, Gutzwiller approximation (GA) electronic structure calculations have the great advantage of coupling extreme LDA-level simplicity with qualitatively, often quantitatively, increased accuracy in the description of correlations. For example, GA has been able to describe conducting materials that are insulators "in disguise" [9], i.e., whose properties depend on correlations that are already present in their Mott insulating phase, and that continue to play an important role even in the nearby metallic phases. Another famous result of the GA is the Brinkman-Rice description of the Mott transition in vanadium sesquioxide, originally derived by the GA solution to the Hubbard model [10]. Because of its simplicity, a great deal of effort has been devoted in recent years to extend GA from simple lattice models to more realistic off-lattice cases [11–20], although there is still a need for a detailed description of the respective protocols. In this paper we begin by presenting in full detail our own implementation of electronic structure calculation exploiting

*giovanni.borghi@epfl.ch
†fabrizio@sissa.it
‡tosatti@sissa.it

the Gutzwiller variational wave function together with the LDA density functional. The Levy-Lieb constrained-search formulation of DFT provides a solid theoretical framework for the introduction of Gutzwiller variational parameters in the density functional, while a localized atomic basis set makes the definition of the Gutzwiller-projected states straightforward. For that scope we choose the SIESTA electronic structure code with a minimal basis, an approximation which does not aim at state-of-the-art accuracy, but which we find suitable for our application. The application which we focus upon is an analysis of the effect of magnetic moment fluctuations in an elemental transition metal, namely the fundamental energy balance behind ferromagnetic long-range order of bcc Fe. While ferromagnetism of Fe is, in fact, one of the most studied problems in electronic structure, with a vast and rich literature [21–27] including very accurate DFT studies as well as previous LDA + Gutzwiller work [12], not all basic questions about the electronic origin of magnetic order have been answered. In the itinerant model, also realized by spin-polarized LDA calculations, the ferromagnetic ordering of iron sets in due to direct intersite exchange. Through magnetic order the electrons can reduce their mutual Coulomb repulsion, naturally at the extra cost of some increase of electron kinetic energy. Reasoning based on an alternative localized viewpoint [28,29] as well as on more recent local density approximation plus dynamical mean-field theory (LDA + DMFT) studies [30,31], however, suggest that orbital-selective correlations might be at play in the ferromagnetic ordering of Fe. If the poorly dispersive e_g-type electrons of metallic Fe became more localized due to interactions and conduction phenomena were restricted within the t_{2g} manifold (besides, of course, the s electrons) [28,32,33], then ferromagnetic alignment might impinge much more on intersite propagation than in the itinerant picture. In a possible extreme example the localized e_g electrons would form spin-1 moments coupled ferromagnetically via an intra-atomic Hund's exchange to the electrons in the nearly full itinerant t_{2g} bands, so that in order to preserve coherent t_{2g} hole motion, the local e_g moments must order ferromagnetically. As in the manganites, ferromagnetism would in that example be driven by a kinetic energy gain rather than a potential energy one. A kinetic energy gain mechanism for ferromagnetism was also proposed by Hirsch [34].

Exploration of this possibility has not been fully pursued so far, and it is what we attempt here. Even though our local density approximation plus Gutzwiller method (LDA + G) approach can only naively address, through a Brinkman-Rice description, dynamical phenomena such as orbital-selective Mott transitions—especially so in a delicate case where the two sets of orbitals, e_g and t_{2g}, hybridize with each other in the Brillouin zone—and despite our deliberate restriction to a minimal basis dictated by the desire to work with agility and to concentrate on evaluating energy balances in a leaner subspace, we find that the detailed analysis of the separate kinetic and potential energy balance in our approximate Gutzwiller implementation actually supports double exchange as the driving mechanism of ferromagnetism in iron, as opposed to the conventional balance expected in the itinerant picture.

The plan of this article is as follows. In Sec. II we introduce the formalism of LDA + G starting from the constrained-search formulation of DFT, demonstrating how the Gutzwiller wave function can be used to generalize the well-known local density approximation plus Hubbard-U (LDA + U) [35,36] approach by allowing the expectation value of the atomic Hamiltonian to be computed on a multideterminant wave function. In Sec. III we then show how the different terms of the LDA + G density functional can be computed by means of GA and how the total energy of a correlated electronic system can be minimized by a three-step iterative procedure. In Sec. IV we finally present and comment in Sec. V the physical results for paramagnetic and ferromagnetic bcc Fe and connect back to the basic questions about the origin of ferromagnetic order.

II. CONSTRAINED-SEARCH FORMULATION OF A GUTZWILLER DENSITY FUNCTIONAL THEORY

The fundamentally based way to introduce a Gutzwiller density functional is through the formalism independently proposed by Levy [37,38] and Lieb [39]. Starting from the Rayleigh-Ritz definition for the ground-state energy $E_{\rm GS}$ of a system,

$$E_{\rm GS} = \min_{\Psi} \langle \Psi | H | \Psi \rangle, \tag{1}$$

where the electron Hamiltonian H includes the kinetic energy T, the electron-electron interaction $V_{\rm ee}$, and a local external potential $V_{\rm ext}$, Levy and Lieb converted the variational principle for the ground-state wave function into a variational principle for the ground-state density through a constrained minimization at fixed density $n(\boldsymbol{r})$,

$$E_{\rm GS}[V_{\rm ext}(\boldsymbol{r})] = \min_{n(\boldsymbol{r})} \left\{ \min_{\Psi \to n(\boldsymbol{r})} \langle \Psi | T + V_{\rm ee} | \Psi \rangle + \int V_{\rm ext}(\boldsymbol{r}) n(\boldsymbol{r}) \right\}. \tag{2}$$

The first term on the right-hand side of (2) is nothing but the constrained-search definition of the Hohenberg-Kohn functional [40], i.e.,

$$F_{\rm HK}[n(\boldsymbol{r})] = \min_{\Psi \to n(\boldsymbol{r})} \langle \Psi | T + V_{\rm ee} | \Psi \rangle, \tag{3}$$

which is independent of the external potential $V_{\rm ext}$. The wave function Ψ in the definition Eq. (3) should span the whole many-body Hilbert space, generally too large to allow for a straightforward numerical evaluation of $F_{\rm HK}[n(\boldsymbol{r})]$. Within the Kohn-Sham scheme, the generality of Eq. (3) is abandoned in favor of a more practical definition of the Hohenberg-Kohn functional, which is split into kinetic, Hartree, and exchange-correlation terms, namely,

$$F_{\rm HK}[n(\boldsymbol{r})] = T_s[n(\boldsymbol{r})] + E_{\rm H}[n(\boldsymbol{r})] + E_{\rm xc}[n(\boldsymbol{r})], \tag{4}$$

where $E_{\rm H}[n(\boldsymbol{r})]$ is the electrostatic energy of the electron density regarded as a classical charge distribution. A constrained search is then retained only for the kinetic contribution,

$$T_s[n(\boldsymbol{r})] = \min_{\Psi \to n(\boldsymbol{r})} \langle \Psi | T | \Psi \rangle, \tag{5}$$

which, because T is a one-body operator, has a solution within the class of Slater determinants, a relatively simple task to accomplish through auxiliary noninteracting electron Hamiltonians whose ground-state local density $n(\boldsymbol{r})$ coincides with that of the physical interacting model. The difficulties of

the original many-body problem have thus been hidden in the unknown exchange-correlation functional $E_{\rm xc}[n(\boldsymbol{r})]$. All DFT approximation schemes correspond to different guesses of a physically sensible functional form of $E_{\rm xc}[n(\boldsymbol{r})]$ in terms of the local density.

The main problem that arises from the density-dependent parametrization Eq. (5) is that $E_{\rm H}[n(\boldsymbol{r})]$ contains a spurious self-interaction (SI) term—finite even when $n(\boldsymbol{r})$ is the density of a single electron—a term which should be identically canceled in the exact $E_{\rm xc}[n(\boldsymbol{r})]$. Unfortunately, all semilocal approximations to $E_{\rm xc}[n(\boldsymbol{r})]$, such as LDA and generalized gradient approximation (GGA), fail to fully subtract the SI term from the density functional. The results thus by construction contain a certain level of self-interaction error, the filled Kohn-Sham one-electron levels being artificially pushed up in energy relative to the empty ones. The spurious SI one-electron energy is larger for spatially localized electronic wave functions. For instance, a single electron with a simple Gaussian wave function feels a SI that is inversely proportional to the standard deviation of the Gaussian, only 70% of which is subtracted by the LDA exchange functional. The improvements attained by better functionals do not seem major [41]. All density-functional calculations are affected to some extent by the SI error, more important when the real-space one-body density matrix is more localized. That is especially the case for most transition metals and transition-metal oxides. In a density functional calculation with semilocal functionals, the spurious SI term acts effectively as a penalty term preventing electron localization, generally spoiling agreement with experimental data for band gaps, magnetization, and other physical observables such as lattice constant and bulk modulus.

A. Review of SIC and LDA + U approximations

A popular way to reduce the SI while still remaining in the context of local or semilocal density functionals is to include in the kinetic functional Eq. (5) part of the electron-electron interaction, specifically the projection $H_{\rm at}$ of $V_{\rm ee}$ on an atomiclike orbital (see below). The common choice is to consider only orbitals that are partially occupied within standard LDA, hence which suffer more from the SI. The noninteracting kinetic functional $T_s[n(\boldsymbol{r})]$ is thus turned into a modified kinetic functional $T_i[n(\boldsymbol{r})]$,

$$T_s[n(\boldsymbol{r})] \to T_i[n(\boldsymbol{r})] = \min_{\Psi_0 \to n(\boldsymbol{r})} \langle \Psi_0 | T + H_{\rm at} | \Psi_0 \rangle, \quad (6)$$

and the Hohenberg and Kohn functional changes into

$$F_{\rm HK}[n(\boldsymbol{r})] = T_i[n(\boldsymbol{r})] + E_{\rm H}[n(\boldsymbol{r})] + E_{\rm xc}[n(\boldsymbol{r})] - E_{\rm dc}[n(\boldsymbol{r})], \quad (7)$$

where $E_{\rm dc}[n(\boldsymbol{r})]$ is a double-counting energy which must cancel the contribution of $H_{\rm at}$ already included within LDA.

In Eq. (6) the constrained search is still restricted to the space of Slater determinants Ψ_0, so that the modified kinetic functional can be dealt with within an independent-particle picture and therefore included in the Kohn-Sham scheme. Essentially, the interaction $H_{\rm at}$ is treated by HF, which—while still unable to capture the Mott localization phenomenon—is devoid of SI, a correlation effect. Further below we discuss how to improve the functional T_i so as to make Mott physics accessible. Here in addition we briefly discuss how to define properly $H_{\rm at}$. Typically, $H_{\rm at} = \sum_{\boldsymbol{R}} H_{\rm at}^{(\boldsymbol{R})}$, with $H_{\rm at}^{(\boldsymbol{R})}$ accounting for the leading-order multipolar expansion of the Coulomb interaction projected onto a selected set of atomiclike orbitals $|\phi_{\boldsymbol{R},m}^{(l)}\rangle$ with angular momentum l at atomic site $\boldsymbol{R}$ in the lattice,

$$\begin{aligned} H_{\rm at}^{(\boldsymbol{R})} = {} & \frac{F_0}{2} N_{\boldsymbol{R}}(N_{\boldsymbol{R}} - 1) + \frac{1}{2} \sum_{L>0}^{2l} F_L \left(C_{l0\,L0}^{l0}\right)^2 \\ & \times \sum_{M=-L}^{L} (-1)^M C_{lm'\,LM}^{lm} C_{lm'_1\,L-M}^{lm_1} \\ & \times c_{\boldsymbol{R},m\sigma}^{\dagger} c_{\boldsymbol{R},m_1\sigma_1}^{\dagger} c_{\boldsymbol{R},m'_1\sigma_1} c_{\boldsymbol{R},m'\sigma}, \end{aligned} \quad (8)$$

where $N_{\boldsymbol{R}}$ is the total electron number operator at site $\boldsymbol{R}$ projected onto the selected set of atomic orbitals, $L = 2n$ with $n = 1, \ldots, l$, $C_{lm'\,LM}^{lm}$ are the Clebsch-Gordan coefficients, and the parameters F_L are known as Slater integrals. The first term on the right-hand side of Eq. (8), which we denote hereafter as $H_{\rm Hub}^{(\boldsymbol{R})}$, is a pure charge repulsion term, its coupling constant F_0 generally called the "Hubbard U". The remaining terms instead enforce Hund's first and second rules; hence, they may be referred to as the Hund's rule exchange ($H_{\rm Hund}$).

The so-called "rotationally invariant LDA + U" method, developed by Lichtenstein and co-workers [42] as a basis-set independent formulation of the LDA + U method by Anisimov, Zaanen, and Andersen [35] is based on the mean-field treatment [Eq. (6)] of the atomic interaction Hamiltonian in Eq. (8). It gives the possibility to improve the description of electron-electron interactions in density functional calculations with no extra requirement of computational resources. The difficulties in using the full expression Eq. (8) as interaction Hamiltonian are twofold. First, one needs a sound recipe for estimating the parameters of the interaction Hamiltonian, which in the case of $l = 2$ are the three Slater integrals F_0, F_2, and F_4. For this purpose, it is common to assume atomic values for the ratio F_4/F_2, an assumption which reduces to two the parameters to choose for the Hamiltonian (8), which are F_0 (the Hubbard U) and $J = (F_2 + F_4)/14$ [43]. The latter can be estimated from DFT [43,44] or can be given atomic values, extracted from tabulated spectroscopic data [45] or quantum chemistry calculations [46]. A second issue associated with the full atomic interaction Hamiltonian (8) is the difficulty of finding a proper expression for electron double counting. The latter should, by definition, be equivalent to the LDA approximation to the atomic interaction energy, Eq. (8). However, that energy depends, in principle, on the specific point symmetry of the system, and one cannot find a general expression valid for every case.

The simplified LDA + U scheme used for the first time by Dudarev [47] includes only the F_0 term in the atomic Hamiltonian. In this simplified approach, mainly two expressions for the double-counting term are available: the "fully localized limit" [48] and "around-mean-field limit" [49]. The first is more suitable for systems with strongly localized electrons, while the second is the best for systems with stronger intersite hybridization of d electrons. The two schemes can be combined together with weight factors [43] to yield optimal

results. Cococcioni and de Gironcoli [50] also provided, for this simplified LDA + U, an *ab initio* procedure to compute the parameter F_0 from linear response theory. When used in conjunction with the fully localized recipe for double counting, the Cococcioni LDA + U correction takes the following form:

$$\langle\Psi_0|H_{\rm at}|\Psi_0\rangle - E_{\rm dc}[n(\boldsymbol{r})] = \frac{U}{2}{\rm Tr}[\hat{n}^{(0)}(1-\hat{n}^{(0)})]. \quad (9)$$

The above term, in which U is computed as the curvature of total energy as a function of a change in number of (typically d) electrons, can be also interpreted as a penalty meant to restore the piecewise linearity of the LDA or PBE total energy vs N curve. The restoration of piecewise linearity is connected to the well-known SI problem inherent to most approximate density functionals. In spite of its simplicity, the correction (9) alone is able to improve the performance of conventional semilocal functionals, such as PBE, for both extended systems and small molecules [51,52]. However, there are numerous situations in which this formulation will not be adequate. It is, for instance, well known that only the spherically averaged strength of the exchange-correlation hole is correctly accounted for by the LDA functional, but not its angular dependence. For this reason one cannot expect that the nonpolar correction of Eq. (9) will be apt to describe systems that display strongly orbital-dependent correlations, as was shown to be the case of body-centered cubic iron [30,31]. Indeed, recent studies on iron pnictides and chalcogenides [53–55] suggest that the orbital selectivity displayed by these iron compounds crucially depends on atomic Hund's rules.

In order to be able to describe correctly Hund's rules in iron, we therefore decided to supplement the nonpolar, "Hubbard" term in Eq. (8) with a simplified expression for the F_2 and F_4 terms, written in terms of many-body observables, in such a way that we can assign them more easily a sensible double-counting correction. Specifically, we assume the simplified expression

$$H_{\rm at} = H_{\rm Hub} + H_{\rm Hund}, \quad (10)$$

with the nonpolar term

$$H_{\rm Hub} = \frac{U}{2}N(N-1) \quad (11)$$

and the exchange interaction

$$H_{\rm Hund} = -J\left\{\mathbf{S}\cdot\mathbf{S} - \frac{3}{4}N + \frac{N(N-1)}{4} + \sum_m n_{m\uparrow}n_{m\downarrow}\right\}, \quad (12)$$

for which we choose a double-counting energy,

$$\begin{aligned} &E_{\rm dc}^{\rm Hub}[n(\boldsymbol{r})] + E_{\rm dc}^{\rm Hund}[n(\boldsymbol{r})] \\ &\quad = \frac{U}{2}N(N-1) \\ &\qquad -J\left[\frac{N_\uparrow(N_\uparrow-1)}{2} + \frac{N_\downarrow(N_\downarrow-1)}{2} + \frac{N_\uparrow N_\downarrow}{2l+1}\right]. \end{aligned} \quad (13)$$

We observe that the first term on the right-hand side of Eq. (12) implements the first Hund's rule, while the last term implements the second rule.

B. Extending LDA + U to LDA + Gutzwiller

The key difference between LDA + G and LDA + U resides in the definition of the modified kinetic functional $T_{\rm i}$. Within LDA + G, the definition Eq. (6) changes to

$$T_{\rm i}[n(\boldsymbol{r})] \to T_{\rm G}[n(\boldsymbol{r})] = \min_{\Psi_{\rm G}\to n(\boldsymbol{r})}\langle\Psi_{\rm G}|T + H_{\rm at}|\Psi_{\rm G}\rangle, \quad (14)$$

where the wave function $|\Psi_{\rm G}\rangle$ is defined as

$$|\Psi\rangle = \mathcal{P}|\Psi_0\rangle = \prod_{\boldsymbol{R}}\mathcal{P}_{\boldsymbol{R}}|\Psi_0\rangle. \quad (15)$$

In the above equation, $|\Psi_0\rangle$ is still a Slater determinant, and the elements of novelty are the operators $\mathcal{P}_{\boldsymbol{R}}$, which are linear transformations acting on the configurational space of a chosen set of local orbitals at lattice site $\boldsymbol{R}$. As in LDA + U, this set of orbitals $\phi_{m,\boldsymbol{R}}$ retains well-defined atomic angular momentum l, m being its projection on a given quantization axis. The operator $\mathcal{P}_{\boldsymbol{R}}$ can be generally written as

$$\mathcal{P}_{\boldsymbol{R}} = \sum_{\Gamma\Gamma'}\Lambda_{\Gamma\Gamma',\boldsymbol{R}}\,|\Gamma,\boldsymbol{R}\rangle\langle\,\Gamma',\boldsymbol{R}|, \quad (16)$$

where $|\Gamma,\boldsymbol{R}\rangle$ denote many-body configurations of electrons occupying the orbitals $\phi_{m,\boldsymbol{R}}$. Differently from LDA + U, the expectation value of the kinetic plus atomic interaction operators will not depend solely on the Slater determinant $|\Psi_0\rangle$, but also on the variational parameters $\Lambda_{\Gamma\Gamma',\boldsymbol{R}}$ that define $\mathcal{P}_{\boldsymbol{R}}$.

Computing exact expectation values on the Gutzwiller wave function for lattices of finite coordination is a task that can be accomplished only numerically, e.g., through variational quantum Monte Carlo [56,57]. For infinite-coordination lattices, an exact expression can be instead computed analytically. There is, in fact, a close connection between the Gutzwiller variational approach in the limit of infinite lattice coordination and dynamical mean-field theory [5]. In that limit, the single-particle self-energy matrix $\Sigma(\epsilon,\boldsymbol{k}) = \Sigma(\epsilon)$ becomes purely local, hence momentum independent. DMFT makes it possible to evaluate exactly $\Sigma(\epsilon)$ by solving an auxiliary Anderson impurity model constructed in such a way as to have the same self-energy as the system of interest. The Gutzwiller variational approach is instead a consistent approximation to the exact solution, which assumes a Fermi-liquid expression $\Sigma(\epsilon) \simeq \Sigma(0) + (1-Z^{-1})\epsilon$, where Z is commonly referred to as the quasiparticle weight. Because of this assumption, the Gutzwiller wave function can describe only states whose elementary excitations are quasiparticles, such as Landau-Fermi liquids and insulators that can be represented through a Slater determinant. However, the additional freedom brought by the parameter Z, whose value is strictly $Z = 1$ within HF and LDA + U, opens the possibility to access strongly correlated metals, $Z \ll 1$, and thus the approach to a Mott transition, where $Z \to 0$. Although DMFT is exact only in the limit of infinite coordination, it is currently used as an approximation in realistic finite-coordination lattices, under the hypothesis that (strong) correlation effects beyond HF are well represented by $\Sigma(\epsilon,\boldsymbol{k}) \simeq \Sigma_{\rm HF}(\boldsymbol{k}) + \Sigma(\epsilon)$, where $\Sigma_{\rm HF}(\boldsymbol{k})$ is the HF self-energy, eventually including frequency-dependent random-phase-like contributions [58], and the correction $\Sigma(\epsilon)$ is momentum independent and can be obtained by DMFT. Under the same assumptions, one can keep using the formal results of the Gutzwiller variational approach, which are

strictly valid only in infinite-coordination lattices, also in finite-coordination ones, an approximation referred to as the Gutzwiller Approximation (GA). In other words, the GA should be better regarded as an approximation to DMFT, when either of them are used in finite-coordination lattices, rather than an approximation to the exact evaluation of expectation values on the Gutzwiller wave function, Eq. (15). This viewpoint, which we underwrite, is our motivation for adopting the GA in combination with LDA + U as an alternative to LDA + DMFT, at the cost of less rigor, but, as we shall show, with gain in simplicity and flexibility.

Expectation values in the Gutzwiller approximation

In order to determine the functional $T_{\rm G}[n(\boldsymbol{r})]$, one should be able to compute expectation values of both many-body on-site operators, such as those contained in $H_{\rm at}$, and off-site single-particle operators, which are present in the definition of the kinetic operator $\hat{T}$. In all that follows, we use the formalism presented in Ref. [59].

First of all, the Slater determinant $|\Psi_0\rangle$ defines the uncorrelated one-body local density matrix $\hat{n}^{(0)}_{\boldsymbol{R}}$ [the same matrix that enters the LDA + U energy correction term Eq. (9)], with elements

$$n^{(0)}_{\boldsymbol{R}m\sigma,\boldsymbol{R}m'\sigma'} = \langle\Psi_0|c^{\dagger}_{\boldsymbol{R},m\sigma}c_{\boldsymbol{R},m'\sigma'}|\Psi_0\rangle, \tag{17}$$

where $c^{\dagger}_{\boldsymbol{R},m\sigma}$ creates a spin-σ electron in orbital $\phi_{m,\boldsymbol{R}}$. The density matrix $\hat{n}^{(0)}_{\boldsymbol{R}}$ is diagonalized by a unitary transformation that turns the original basis of operators $c^{\dagger}_{\boldsymbol{R},m\sigma}$ into the natural basis of operators $c^{\dagger}_{\boldsymbol{R},\gamma\sigma}$, assuming invariance with respect to spin rotations around the z axis. In the natural basis, the one-body density matrix is therefore diagonal, with eigenvalues $n^{(0)}_{\boldsymbol{R},\gamma\sigma}$. In the natural-orbital Fock basis, with states

$$|\{n_{\boldsymbol{R},\gamma\sigma}\}\rangle \equiv \prod_{\gamma\sigma}(c^{\dagger}_{\boldsymbol{R},\gamma\sigma})^{n_{\boldsymbol{R},\gamma\sigma}}\,|0\rangle,$$

it follows that the probability matrix with elements

$$\begin{aligned} P^{(\boldsymbol{R})}_{0,\{n_{\boldsymbol{R},\gamma\sigma}\}\{m_{\boldsymbol{R},\gamma\sigma}\}} &\equiv \langle\Psi_0|\,|\{m_{\boldsymbol{R},\gamma\sigma}\}\rangle\langle\{n_{\boldsymbol{R},\gamma\sigma}\}|\,|\Psi_0\rangle \\ &= P^{(\boldsymbol{R})}_{0,\{n_{\boldsymbol{R},\gamma\sigma}\}}\,\delta_{\{n_{\boldsymbol{R},\gamma\sigma}\}\{m_{\boldsymbol{R},\gamma\sigma}\}} \\ &= \prod_{\gamma\sigma}\left(n^{(0)}_{\boldsymbol{R},\gamma\sigma}\right)^{n_{\boldsymbol{R},\gamma\sigma}}\left(1-n^{(0)}_{\boldsymbol{R},\gamma\sigma}\right)^{1-n_{\boldsymbol{R},\gamma\sigma}} \end{aligned} \tag{18}$$

is diagonal, too. It is actually convenient [59] to rewrite the operator Eq. (16) in a mixed-basis representation as

$$\mathcal{P}_{\boldsymbol{R}} = \sum_{\Gamma\{n_{\boldsymbol{R},\gamma\sigma}\}}\left(\frac{\Phi_{\Gamma\{n_{\boldsymbol{R},\gamma\sigma}\},\boldsymbol{R}}}{\sqrt{P^{(\boldsymbol{R})}_{0,\{n_{\boldsymbol{R},\gamma\sigma}\}}}}\right)|\Gamma,\boldsymbol{R}\rangle\langle\{n_{\boldsymbol{R},\gamma\sigma}\}|, \tag{19}$$

where $|\Gamma,\boldsymbol{R}\rangle$ is a state, e.g., a Fock state, in the original basis, whereas $|\{n_{\boldsymbol{R},\gamma\sigma}\}\rangle$ is a Fock state in the natural basis. This mixed representation simplifies considerably the calculations. In order to use the GA, we need to impose the two following constraints on the matrix $\hat{\Phi}_{\boldsymbol{R}}$ with elements $\Phi_{\Gamma\{n_{\boldsymbol{R},\gamma\sigma}\},\boldsymbol{R}}$ [59],

$$\mathrm{Tr}\{\hat{\Phi}^{\dagger}_{\boldsymbol{R}}\hat{\Phi}_{\boldsymbol{R}}\} = 1, \tag{20}$$

$$\mathrm{Tr}\{\hat{\Phi}^{\dagger}_{\boldsymbol{R}}\hat{\Phi}_{\boldsymbol{R}}\hat{c}^{\dagger}_{\boldsymbol{R},\gamma\sigma}\hat{c}_{\boldsymbol{R},\gamma'\sigma'}\} = n^{(0)}_{\boldsymbol{R},\gamma\sigma}\delta_{\gamma\gamma'}\,\delta_{\sigma\sigma'}, \tag{21}$$

where $\hat{c}^{\dagger}_{\boldsymbol{R},\gamma\sigma}$ is the matrix representation of the Fermi operator in its Fock basis. If these constraints are fulfilled, then within the GA, which we recall is exact for infinite-coordination lattices, we have

$$\langle\Psi_{\rm G}|\hat{O}_{\boldsymbol{R}}|\Psi_{\rm G}\rangle = \mathrm{Tr}\{\hat{\Phi}^{\dagger}_{\boldsymbol{R}}\hat{O}_{\boldsymbol{R}}\hat{\Phi}_{\boldsymbol{R}}\}, \tag{22}$$

where $\hat{O}_{\boldsymbol{R}}$ is the matrix representation of any local operator. The intersite density matrix can be computed from

$$\begin{aligned} &\langle\Psi_{\rm G}|c^{\dagger}_{\boldsymbol{R},m\sigma}c_{\boldsymbol{R},m'\sigma}|\Psi_{\rm G}\rangle \\ &\quad= \sum_{\gamma\gamma'}R^{\dagger}_{\gamma m;\sigma,\boldsymbol{R}}\,R_{m'\gamma';\sigma,\boldsymbol{R}'}\langle\Psi_0|c^{\dagger}_{\boldsymbol{R},\gamma\sigma'}c_{\boldsymbol{R}',\gamma'\sigma'}|\Psi_0\rangle, \end{aligned} \tag{23}$$

where

$$R^{\dagger}_{\gamma m,\sigma,\boldsymbol{R}} = \frac{\mathrm{Tr}\{\hat{\Phi}^{\dagger}_{\boldsymbol{R}}\,\hat{c}^{\dagger}_{\boldsymbol{R},m\sigma}\,\hat{\Phi}_{\boldsymbol{R}}\,\hat{c}_{\boldsymbol{R},\gamma\sigma}\}}{\sqrt{n^{(0)}_{\boldsymbol{R},\gamma\sigma}\left(1-n^{(0)}_{\boldsymbol{R},\gamma\sigma}\right)}} \tag{24}$$

can be regarded as a wave-function renormalization matrix. Here $\hat{c}^{\dagger}_{\boldsymbol{R},m\sigma}$ is the matrix representation of the original operators in the basis of states $|\Gamma,\boldsymbol{R}\rangle$. When this is the Fock basis constructed by the same original operators, their matrix representation is actually independent of the basis of single-particle wave functions which they refer to; hence, it is the same as for the $\hat{c}^{\dagger}_{\boldsymbol{R},\gamma\sigma}$ operators of the natural basis. In reality, in most cases that are relevant for real materials the natural basis that diagonalizes the local density matrix is determined fully by the lattice symmetry; hence, it is possible and convenient to write the Hamiltonian directly in that basis. In the above formulas, this corresponds to identifying the set of labels $\{m\}$ with $\{\gamma\}$. Since the natural basis is such both for the uncorrelated on-site density matrix,

$$\begin{aligned} n^{(0)}_{\boldsymbol{R}m\sigma,m'\sigma'} &= \langle\Psi_0|c^{\dagger}_{\boldsymbol{R},m\sigma}c_{\boldsymbol{R},m'\sigma'}|\Psi_0\rangle \\ &= \mathrm{Tr}\{\hat{\Phi}^{\dagger}_{\boldsymbol{R}}\,\hat{\Phi}_{\boldsymbol{R}}\,\hat{c}^{\dagger}_{\boldsymbol{R},m\sigma}\hat{c}_{\boldsymbol{R},m'\sigma}\} \\ &= \delta_{mm'}\,n^{(0)}_{\boldsymbol{R},m\sigma}, \end{aligned} \tag{25}$$

and for the correlated one,

$$\begin{aligned} n_{\boldsymbol{R}m\sigma,m'\sigma'} &= \langle\Psi_{\rm G}|c^{\dagger}_{\boldsymbol{R},m\sigma}c_{\boldsymbol{R},m'\sigma'}|\Psi_{\rm G}\rangle \\ &= \mathrm{Tr}\{\hat{\Phi}^{\dagger}_{\boldsymbol{R}}\,\hat{c}^{\dagger}_{\boldsymbol{R},m\sigma}\hat{c}_{\boldsymbol{R},m'\sigma}\,\hat{\Phi}_{\boldsymbol{R}}\} \\ &= \delta_{mm'}\,n_{\boldsymbol{R},m\sigma}, \end{aligned} \tag{26}$$

generally with different eigenvalues, it is not difficult to realize that the wave-function renormalization matrix Eq. (24) becomes diagonal; i.e.,

$$R^{\dagger}_{m'm,\sigma,\boldsymbol{R}} = \frac{\mathrm{Tr}\{\hat{\Phi}^{\dagger}_{\boldsymbol{R}}\,\hat{c}^{\dagger}_{\boldsymbol{R},m\sigma}\,\hat{\Phi}_{\boldsymbol{R}}\,\hat{c}_{\boldsymbol{R},m'\sigma}\}}{\sqrt{n^{(0)}_{\boldsymbol{R},m'\sigma}\left(1-n^{(0)}_{\boldsymbol{R},m'\sigma}\right)}} = \delta_{mm'}\,R^{\dagger}_{m\sigma,\boldsymbol{R}}. \tag{27}$$

The Eqs. (22)–(27) are the basic formulas that make it possible to evaluate the average value of the Hamiltonian as a functional of the Slater determinant and of the matrices $\hat{\Phi}_{\boldsymbol{R}}$, hence to solve the variational problem. The symmetries of every specific system under study can be imposed on the matrices $\hat{\Phi}_{\boldsymbol{R}}$ so as to decrease, in some cases quite drastically, the total number of Gutzwiller parameters (see Appendixes A and B for details).

III. THE GUTZWILLER FUNCTIONAL IN PRACTICE

In this section we show how to perform a LDA + G calculation on a realistic system, namely bcc Fe, which, as mentioned in the Introduction, although a basic and supposedly simple system, still exhibits controversial aspects.

We first have to select the *correlated* orbitals to be treated by the Gutzwiller operator. In the present case the choice is simple: the $3d$ orbitals of Fe. This case is one of those mentioned earlier in which the natural basis is determined by symmetry and corresponds to the cubic crystal field split d orbitals, namely, the e_g doublet and the t_{2g} triplet. In this representation the formulas Eqs. (25)–(27) hold, which is a great simplification. Furthermore, since bcc is a Bravais lattice, the positions $\boldsymbol{R}$ of Fe atoms also label unit cells; hence, by translational symmetry we can safely assume that the variational matrix parameters $\hat{\Phi}_{\boldsymbol{R}} = \hat{\Phi}$ are independent of $\boldsymbol{R}$. So are, therefore, the eigenvalues of the local density matrices, $n^{(0)}_{\boldsymbol{R},m\sigma} = n^{(0)}_{m\sigma}$ and $n_{\boldsymbol{R},m\sigma} = n_{m\sigma}$, as well as the wave-function renormalization $R_{m\sigma,\boldsymbol{R}} = R_{m\sigma}$. To lighten notations, in what follows the orbital labels m refer both to the correlated set and to the uncorrelated ones, unaffected by the action of the Gutzwiller operator. In the last paragraph of this section we come back to this point.

We define the Gutzwiller density functional as

$$\mathcal{F}[n(\boldsymbol{r})] = \min_{\Psi_{\rm G}\to n(\boldsymbol{r})} \mathcal{E}[\Psi_{\rm G}, n(\boldsymbol{r})], \tag{28}$$

where the quantity $\mathcal{E}[\Psi_{\rm G}, n(\boldsymbol{r})]$ undergoing constrained minimization is

$$\begin{aligned}\mathcal{E}[\Psi_{\rm G}, n(\boldsymbol{r})] = {} & \langle \Psi_{\rm G}|T + H_{\rm at}|\Psi_{\rm G}\rangle \\ & + \int V_{\rm ext}(\boldsymbol{r}) n(\boldsymbol{r}) d\boldsymbol{r} \; + \tilde{E}_{\rm H}[n(\boldsymbol{r})] \\ & + \tilde{E}_{\rm xc}[n(\boldsymbol{r})] - E_{\rm dc}[n(\boldsymbol{r})].\end{aligned} \tag{29}$$

For our purposes, it is convenient to rewrite Eq. (28) as a minimization constrained with respect to the "uncorrelated" density $n^{(0)}(\boldsymbol{r})$,

$$\mathcal{F}[n^{(0)}(\boldsymbol{r})] = \min_{\mathcal{P},\Psi_0\to n^{(0)}(\boldsymbol{r})} \mathcal{E}[\Psi_0, \mathcal{P}, n^{(0)}(\boldsymbol{r})], \tag{30}$$

where $\mathcal{E}[\Psi_0, \mathcal{P}, n^{(0)}(\boldsymbol{r})] = \mathcal{E}[\Psi_{\rm G}(\Psi_0, \mathcal{P}), n(\Psi_0, \mathcal{P})]$. The dependence of the "correlated" density $n(\boldsymbol{r})$ upon the "uncorrelated" density $n^{(0)}(\boldsymbol{r})$ can be made explicit once one writes them in terms of the one-body correlated density matrix of the periodic system

$$D_{mm',\sigma,\boldsymbol{R}} = \langle \Psi_{\rm G}| c^\dagger_{\boldsymbol{R},m\sigma} c_{\boldsymbol{0},m'\sigma} |\Psi_{\rm G}\rangle \tag{31}$$

and of the "uncorrelated" density-matrix

$$D^{(0)}_{mm',\sigma,\boldsymbol{R}} = \langle \Psi_0| c^\dagger_{\boldsymbol{R},m\sigma} c_{\boldsymbol{0},m'\sigma} |\Psi_0\rangle, \tag{32}$$

namely,

$$\begin{aligned} n^{(0)}(\boldsymbol{r}) &= \sum_\sigma n^{(0)}_\sigma(\boldsymbol{r}) \\ &= \sum_{m,m',\sigma,\boldsymbol{R}} D^{(0)}_{mm',\sigma,\boldsymbol{R}} \, \phi^*_{m,\boldsymbol{R}}(\boldsymbol{r}) \, \phi_{m',\boldsymbol{0}}(\boldsymbol{r}), \end{aligned} \tag{33}$$

$$\begin{aligned} n(\boldsymbol{r}) &= \sum_\sigma n_\sigma(\boldsymbol{r}) \\ &= \sum_{m,m',\sigma,\boldsymbol{R}} D_{mm',\sigma,\boldsymbol{R}} \, \phi^*_{m,\boldsymbol{R}}(\boldsymbol{r}) \, \phi_{m',\boldsymbol{0}}(\boldsymbol{r}). \end{aligned} \tag{34}$$

Indeed, $D_{mm',\sigma,\boldsymbol{R}}$ can be obtained by $D^{(0)}_{mm',\sigma,\boldsymbol{R}}$ using the recipe of the GA,

$$D_{mm',\sigma,\boldsymbol{R}} = \begin{cases} R^\dagger_{m\sigma} \, D^{(0)}_{mm',\sigma,\boldsymbol{R}} \, R_{m'\sigma}, & \boldsymbol{R} \neq \boldsymbol{0}, \\ {\rm Tr}\left\{\hat{\Phi}^\dagger \, \hat{n}_{mm',\sigma} \, \hat{\Phi}\right\} = \delta_{mm'} n_{m\sigma}, & \boldsymbol{R} = \boldsymbol{0}, \end{cases} \tag{35}$$

where $\hat{n}_{mm',\sigma}$ is the matrix representation on the local Fock space at site $\boldsymbol{R}$ of $c^\dagger_{\boldsymbol{R},m\sigma} c_{\boldsymbol{R},m'\sigma}$, which is independent of $\boldsymbol{R}$ for a periodic system, and where $n_{m\sigma}$ is equal to $n_{\boldsymbol{R}=0,m\sigma}$ defined in Eq. (26).

In order to write $\mathcal{E}[\Psi_0, \mathcal{P}, n^{(0)}(\boldsymbol{r})]$ explicitly in terms of the new variables, we start from the first and second terms of Eq. (29). We can now treat the kinetic and the external potential terms on the same footing through

$$\begin{aligned} & \langle \Psi_{\rm G}|T|\Psi_{\rm G}\rangle + \int n(\boldsymbol{r}) V_{\rm ext}(\boldsymbol{r}) d\boldsymbol{r} \\ & \quad = \sum_{m,m',\sigma,\boldsymbol{R}} \left(T_{mm',\boldsymbol{R}} + V^{\rm (ext)}_{mm',\boldsymbol{R}}\right) D_{mm',\sigma,\boldsymbol{R}}, \end{aligned} \tag{36}$$

where values of $T_{mm',\boldsymbol{R}}$ and $V^{\rm (ext)}_{mm',\boldsymbol{R}}$ are the spin-independent matrix elements of the kinetic and external potential operators computed between our basis orbitals at sites $\boldsymbol{R}$ and $\boldsymbol{0}$, i.e.,

$$V^{\rm (ext)}_{mm',\boldsymbol{R}} = \int \phi^*_{m,\boldsymbol{R}}(\boldsymbol{r}) V_{\rm ext}(\boldsymbol{r}) \phi_{m',\boldsymbol{0}}(\boldsymbol{r}) d\boldsymbol{r}, \tag{37}$$

$$T_{mm',\boldsymbol{R}} = -\frac{\hbar^2}{2m} \int \phi^*_{m,\boldsymbol{R}}(\boldsymbol{r}) [\nabla^2 \phi_{m',\boldsymbol{0}}(\boldsymbol{r})] d\boldsymbol{r}, \tag{38}$$

and compute the value of the atomic interaction energy $\langle \Psi_{\rm G}|H_{\rm at}|\Psi_{\rm G}\rangle$ using the GA recipe,

$$E_{\rm at}[\Psi_0, \mathcal{P}] = \langle \Psi_{\rm G}|H_{\rm at}|\Psi_{\rm G}\rangle = {\rm Tr}\{\hat{\Phi}^\dagger \hat{H}_{\rm at} \hat{\Phi}\}. \tag{39}$$

In order to simplify the density self-consistent LDA + G minimization we decided to use the Hartree $\tilde{E}_{\rm H}[n(\boldsymbol{r})]$ and exchange-correlation $\tilde{E}_{\rm xc}[n(\boldsymbol{r})]$ functionals as the LDA functionals linearized around the uncorrelated density $n^{(0)}(\boldsymbol{r})$. We checked *a posteriori* the accuracy of such a linearization. The modified Hartree functional then reads

$$\begin{aligned} \tilde{E}_{\rm H}[n^{(0)}(\boldsymbol{r}), n(\boldsymbol{r})] \simeq {} & \frac{e^2}{2} \int d\boldsymbol{r} d\boldsymbol{r}' \, \frac{n^{(0)}(\boldsymbol{r}) n^{(0)}(\boldsymbol{r}')}{|\boldsymbol{r} - \boldsymbol{r}'|} \\ & + \int d\boldsymbol{r} \, \delta n(\boldsymbol{r}) \, v_{\rm H}[n^{(0)}(\boldsymbol{r})], \end{aligned} \tag{40}$$

where $\delta n(\boldsymbol{r}) = \sum_\sigma \delta n_\sigma(\boldsymbol{r}) = \sum_\sigma n_\sigma(\boldsymbol{r}) - n^{(0)}_\sigma(\boldsymbol{r})$ and $v_{\rm H}[n^{(0)}(\boldsymbol{r})]$ is the conventional Hartree potential, whereas the exchange-correlation functional is

$$\begin{aligned} \tilde{E}_{\rm xc}[n^{(0)}(\boldsymbol{r}), n(\boldsymbol{r})] = {} & \sum_\sigma \int d\boldsymbol{r} \, n^{(0)}_\sigma(\boldsymbol{r}) \, \epsilon_{{\rm xc},\sigma}[n^{(0)}(\boldsymbol{r})] \\ & + \int d\boldsymbol{r} \, v_{{\rm xc},\sigma}[n^{(0)}(\boldsymbol{r})] \, \delta n_\sigma(\boldsymbol{r}), \end{aligned} \tag{41}$$

$v_{xc}[n^{(0)}(\boldsymbol{r})]$ being the LDA exchange-correlation potential. Note that the choice of $\tilde{E}_H$ involves neglecting a term,

$$\Delta E_H[n^{(0)}(\boldsymbol{r}),n(\boldsymbol{r})] = \tilde{E}_H[n^{(0)}(\boldsymbol{r}),n(\boldsymbol{r})] - E_H[n(\boldsymbol{r})] = \frac{e^2}{2}\int d\boldsymbol{r}d\boldsymbol{r}'\,\frac{\delta n(\boldsymbol{r})\delta n(\boldsymbol{r}')}{|\boldsymbol{r}-\boldsymbol{r}'|}, \quad (42)$$

which can be interpreted as the energy of correlation-induced charge fluctuations. This term, together with the corresponding one neglected for the exchange-correlation functional, $\Delta E_{xc}[n^{(0)}(\boldsymbol{r}),n(\boldsymbol{r})]$, can be computed at the end of the LDA + G calculation in order to provide an estimate of the error due to approximations (40) and (41) (see Table VI). It is worth mentioning that the linearization (41) of exchange-correlation energy around the "uncorrelated" density does not spoil the sum rule for the LDA exchange-correlation hole. As for the double-counting term, similarly to what is done within LDA + U, it is chosen as a function of the local "uncorrelated" density-matrix $n^{(0)}$ only, $E_{dc}[n(\boldsymbol{r})] = E_{dc}[n^{(0)}]$.

A. Three-step minimization of the LDA + Gutzwiller functional

The two densities $n(\boldsymbol{r})$ and $n^{(0)}(\boldsymbol{r})$ must be such that Gutzwiller constraints are fulfilled. In our case where original and natural bases coincide, the constraints on the density matrix can be written as

$$D^{(0)}_{mm',\sigma,\boldsymbol{R}=\boldsymbol{0}} = n^{(0)}_{m\sigma}\,\delta_{mm'}, \quad (43)$$

$$\mathrm{Tr}\{\hat{\Phi}^\dagger\hat{\Phi}\;\hat{n}_{mm',\sigma}\} = n^{(0)}_{m\sigma}\,\delta_{mm'}, \quad (44)$$

where we regard $n^{(0)}_{m\sigma}$ as an additional independent variational parameter of the density functional. These constraints can be enforced with Lagrange multipliers, together with the first Gutzwiller constraint

$$\mathrm{Tr}\{\hat{\Phi}^\dagger\hat{\Phi}\} = 1. \quad (45)$$

Summing up all contributions and adding the electrostatic ion-ion interaction E_{ion}, we find that the overall functional we need to minimize has the form

$$\mathcal{F}\left[n(\boldsymbol{r}),n^{(0)}(\boldsymbol{r}),n^{(0)}_{m\sigma}\right] = \max_{\lambda\lambda'\lambda_0}\Big[\mathcal{K}[n(\boldsymbol{r})] + E_{at}[n(\boldsymbol{r})] - E_{dc}\left[n^{(0)}_{m\sigma}\right] + E^{(0)}_H[n^{(0)}(\boldsymbol{r})] + E^{(0)}_{xc}[n^{(0)}(\boldsymbol{r})] - \lambda_0(\mathrm{Tr}\{\hat{\Phi}^\dagger\hat{\Phi}\}-1) - \sum_{mm'\sigma}\lambda'_{mm',\sigma}\left(D^{(0)}_{mm',\sigma,\boldsymbol{R}=\boldsymbol{0}} - n^{(0)}_{m\sigma}\delta_{mm'}\right) - \lambda_{mm',\sigma}\left(\mathrm{Tr}\{\hat{\Phi}^\dagger\hat{\Phi}\;\hat{n}_{mm',\sigma}\} - n^{(0)}_{m\sigma}\delta_{mm'}\right)\Big] + E_{ion}, \quad (46)$$

where the functional $\mathcal{K}[n(\boldsymbol{r})]$ contains all terms which depend on $n(\boldsymbol{r})$ linearly through the renormalized density matrix D, namely,

$$\mathcal{K}(D) = \sum_{mm',\sigma,\boldsymbol{R}}\left[T_{mm',\boldsymbol{R}} + V^{(H)}_{mm',\boldsymbol{R}} + V^{(xc)}_{mm',\sigma,\boldsymbol{R}} + V^{(ext)}_{mm',\boldsymbol{R}}\right] \times D_{mm',\sigma,\boldsymbol{R}} \equiv \sum_{mm',\sigma,\boldsymbol{R}}\mathcal{K}_{mm',\sigma,\boldsymbol{R}}\,D_{mm',\sigma,\boldsymbol{R}}, \quad (47)$$

where $V^{(H)}_{mm',\boldsymbol{R}}$ and $V^{(xc)}_{mm',\sigma,\boldsymbol{R}}$ are the matrix elements of v_H and v_{xc} between basis orbitals, respectively. For every fixed value of $n^{(0)}_{m\sigma}$, we can optimize $\mathcal{F}$ with respect to the two densities $n^{(0)}(\boldsymbol{r})$ and $n(\boldsymbol{r})$. In practice, by inspection of Eqs. (33)–(35) one can see that this is equivalent to a minimization with respect to the Slater determinant $|\Psi_0\rangle$ and the Gutzwiller parameters contained in the operator $\hat{\Phi}$. This minimization can be carried out in two separate steps.

(1) First, carry out a SIESTA self-consistent calculation to find the Slater determinant Ψ_0 that optimizes $\mathcal{F}[n(\boldsymbol{r}),n^{(0)}(\boldsymbol{r}),n^{(0)}_{m\sigma}]$ with respect to $n^{(0)}(\boldsymbol{r})$, enforcing the constraint (43) through an augmented Lagrangian method [60]. The Gutzwiller parameters, and therefore the hopping renormalization parameters $R_{m\sigma}$, are kept fixed throughout this optimization. The atomic energy $E_{at}[n(\boldsymbol{r})]$ does not change; nor does the double-counting energy $E_{dc}[n^{(0)}(\boldsymbol{r})]$, which is a function of $n^{(0)}(\boldsymbol{r})$ only through $n^{(0)}_{m\sigma}$. The self-consistent single-particle Kohn-Sham equations allowing the minimization with respect to $|\Psi_0\rangle$ are

$$\sum_{m'\boldsymbol{R}}\mathcal{H}_{mm',\sigma,\boldsymbol{R}}\,\psi_{m'\sigma,\boldsymbol{R}} = \varepsilon\,\psi_{m,\sigma,\boldsymbol{0}}, \quad (48)$$

where

$$\mathcal{H}_{mm',\sigma,\boldsymbol{R}} = \mathcal{K}_{mm',\sigma,\boldsymbol{R}} + V^{(0)}_{mm',\sigma,\boldsymbol{R}} - \lambda'_{mm',\sigma}\delta_{\boldsymbol{R}\boldsymbol{0}},$$

and

$$V^{(0)}_{mm',\sigma,\boldsymbol{R}} = \int d\boldsymbol{r}\,\phi^*_{m,\boldsymbol{R}}(\boldsymbol{r})\{v_H[n^{(0)}(\boldsymbol{r})] + v_{xc}[n^{(0)}(\boldsymbol{r})]\} \times \phi_{m',\boldsymbol{0}}(\boldsymbol{r}). \quad (49)$$

(2) Next, optimize $\mathcal{F}$ with respect to Gutzwiller parameters by a Lanczos-improved Levenberg-Marquardt (LM) algorithm (see Appendix C), enforcing the constraints (44) and (45). During this optimization, only the term $\mathcal{K}[n(\boldsymbol{r})]$ and the atomic energy $E_{at}[n(\boldsymbol{r})]$ in Eq. (46) are modified. These two quantities, together with the terms enforcing constraints for Gutzwiller parameters, build a quartic functional $F_{\hat{\Phi}}$ of the matrices $\hat{\Phi}$, with explicit form

$$F_{\hat{\Phi}} = \sum_{m,m',\sigma}\Big[\mathcal{K}_{mm',\sigma,\boldsymbol{R}=\boldsymbol{0}}\,\mathrm{Tr}\{\hat{\Phi}^\dagger\hat{n}_{mm',\sigma}\hat{\Phi}\} + R^\dagger_{m\sigma}\tau_{mm',\sigma}R_{m'\sigma} + \mathrm{Tr}\{\hat{\Phi}^\dagger\hat{H}_{at}\hat{\Phi}\} - \lambda_{mm',\sigma}\left(\mathrm{Tr}\{\hat{\Phi}^\dagger\hat{\Phi}\hat{n}_{mm',\sigma}\} - n^{(0)}_{m\sigma}\delta_{mm'}\right) - \lambda_0(\mathrm{Tr}\{\hat{\Phi}^\dagger\hat{\Phi}\}-1)\Big], \quad (50)$$

where $\tau_{mm',\sigma}$ is

$$\tau_{mm',\sigma} = \sum_{\boldsymbol{R}\neq 0,mm'} \mathcal{K}_{mm',\sigma,\boldsymbol{R}}\, D^{(0)}_{mm',\sigma,\boldsymbol{R}}. \tag{51}$$

These two steps are repeated one after the other until self-consistency is achieved over both densities $n(\boldsymbol{r})$ and $n^{(0)}(\boldsymbol{r})$. Once converged, we are left with a total energy functional depending on the diagonal matrix elements $n^{(0)}_{m\sigma}$, and that can be optimized by steepest descent, so as to fulfill the stationary equations

$$\frac{\partial \mathcal{K}[n(\boldsymbol{r})]}{\partial n^{(0)}_{m\sigma}} - \frac{\partial E_{\rm dc}[n^{(0)}(\boldsymbol{r})]}{\partial n^{(0)}_{m\sigma}} + \lambda_{mm,\sigma} + \lambda'_{mm,\sigma} = 0. \tag{52}$$

The terms appearing in the above equations are the only ones depending on the local uncorrelated density matrix $n^{(0)}_{m\sigma}$. The double-counting energy is a function of this density matrix only, while the functional $\mathcal{K}$, containing the renormalized density matrix $D_{mm',\sigma,\boldsymbol{R}}$, depends on $n^{(0)}_{m\sigma}$ through the wave-function renormalization parameters $R_{m\sigma}$.

B. Atomic basis-set angular momentum-dependent renormalization for transition metals

Equations (31) and (32) describe a density matrix on a basis of orthogonalized atomic orbitals. For a system described by a single set of atomic d orbitals, the indices m and m' are allowed to run on every value of the magnetic quantum number, $m = \{-2,-1,0,1,2\}$. For a cubic system, the basis which diagonalizes the one-body density matrix $D_{\boldsymbol{R},mm'}$ for $\boldsymbol{R} = 0$ is the basis of d orbitals which have real harmonics as their angular part, so that $m = \{r^2-3z^2, x^2-y^2, xy, xz, yz\}$, or in the language of group representations, $m = \{e_g^{(1)}, e_g^{(2)}, t_{2g}^{(1)}, t_{2g}^{(2)}, t_{2g}^{(3)}\}$. In general, simulating the electronic structure of a transition metal with an atomic basis set, such as the SIESTA code does, will require also s orbitals to be present in the set, as well as p orbitals, all of them being hybridized due to the cubic crystal field. We need therefore to reframe Eq. (35) by adding an additional couple of indices $l = 0,1$ besides $l = 2$. Assuming for simplicity that Gutzwiller renormalization affects only d-type orbitals, we have that

$$D_{lm\,l'm',\sigma,\boldsymbol{R}} = R^{l\dagger}_{m\sigma}\, D^{(0)}_{lm\,l'm',\sigma,\boldsymbol{R}}\, R^{l'}_{m'\sigma}, \tag{53}$$

with

$$R^{l}_{m\sigma} = \begin{cases} R_{m\sigma}; & l = 2, \\ 1; & l = 1,0, \end{cases} \tag{54}$$

for the $\boldsymbol{R} \neq 0$ part, and

$$D_{lm\,l'm',\sigma,\boldsymbol{R}=0} = \begin{cases} D^{(0)}_{lm\,l'm',\sigma,\boldsymbol{R}=0}; & l \neq 2, l' \neq 2, \\ \delta_{ll'} n_{m\sigma}; & l = 2, \end{cases} \tag{55}$$

with $n_{m\sigma} = \mathrm{Tr}\{\hat{\Phi}^\dagger \hat{n}_{mm',\sigma} \Phi\}$, for the on-site $\boldsymbol{R} = 0$ part. In what follows the matrices D and n without angular momentum indices refer to the density matrices of the subset of orbitals with $l = 2$. For any value of l, we assume the indices m and m' to run on the cubic harmonics for that value of l, which ensures the $\boldsymbol{R} = 0$ one-body density matrix to be diagonal, or, in other words, "natural".

The SIESTA code provides also the possibility to use a double set of d-type orbitals together with one set of s and one set of p. The use of two sets of d orbitals (double-ζ basis set), as opposed to a single set (single ζ) is particularly indicated for GGA calculations, in which small changes in the density profile of electrons lying close to the Fermi energy can affect the calculation of the energy much more than in LDA. While the first d-type basis set is more atomiclike and more suited for an LDA + U or LDA + G calculation, the second d-type set has a larger spread, since it is meant to describe better also the tails of the density distribution. For LDA + G calculations we therefore adopt a single-ζ basis set. The same basis set is used for all SIESTA LDA calculations with which we compare our results, both in tables and in graphs. Conversely, we use a double-ζ basis set for all SIESTA GGA calculations whose results we report in this paper.

Should one wish to push LDA + G calculations to a higher level of accuracy—as would be required, e.g., for direct numerical comparison with some of the extremely accurate LDA calculations of ferromagnetic Fe present in the literature, such as the one of Ref. [25]—one should, of course, use a more extended basis set in the LDA + G calculation as well. For our more limited scopes, however, the single-ζ basis set, although imperfect, is more than suitable to explore the method and the main physical features we are looking for. The approximation is all the more reasonable given the presently limited quantitative knowledge of the electron-electron interaction parameters U and J that characterize the treatment of correlations at any level of accuracy, as well as the issue of a proper definition of the double-counting term.

IV. RESULTS

In this section we show our results obtained with the previously explained implementation of LDA + G in the SIESTA code. In all SIESTA results that follow, we used the LDA functional parametrized from the data of Ceperley and Alder [61], a $10 \times 10 \times 10$ Monkhorst-Pack k-point grid [62], a real-space mesh (for the representation of the density) cutoff of 150 Ry and a Fermi-Dirac smearing of 20 meV.

A. Nonmagnetic iron

In order to assess the effect of Gutzwiller renormalization parameters Φ on the eigenvalues of the single-particle Kohn-Sham Hamiltonian at density self-consistency, we started by calculating nonmagnetic Fe. Figure 1 shows the band structure of nonmagnetic (spin unpolarized) iron for different values of interaction parameters U and J in the atomic Hamiltonian

$$H_{\rm at} = \frac{U}{2} N(N-1) - J\, \mathbf{S}\cdot\mathbf{S} - \kappa\, \mathbf{L}\cdot\mathbf{L}, \tag{56}$$

where the parameter κ has been added in order to single out the effect of Hund's third rule. The value of $\kappa \approx 0.2$ eV is estimated from spectroscopic data of Corliss and Sugar [45]. A reasonable value of $J = 1.2$ eV can be obtained from spectroscopic data, a value which is very similar to the one expressed in terms of Slater atomic integrals F_2 and F_4, calculated using the electronic structure program by Cowan [63]. The band structures plotted in Fig. 1 are obtained by performing only the first and second optimization steps as

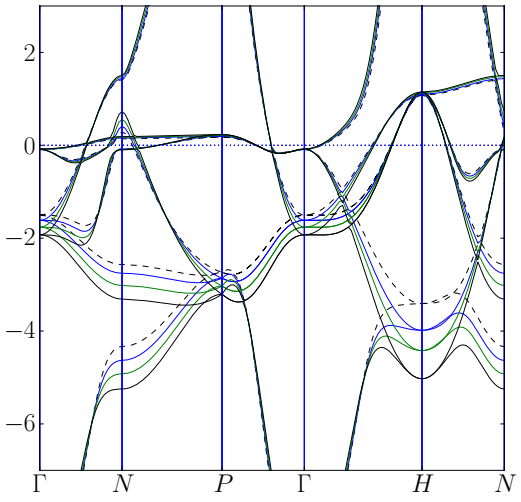

FIG. 1. (Color online) Band structure results for a SIESTA LDA + G calculation of nonmagnetic bcc iron without optimization of the natural density matrix $n^{(0)}_{m\sigma}$. The atomic interaction Hamiltonian we used is displayed in Eq. (56), and the values for its parameters are listed in Table I. The black solid line corresponds to $U = 0$ and $J = 0$, the green line to $U = 5$, $J = 1.2$, the blue line to $U = 10$, $J = 1.2$, and the dashed line to $U = 10$ and $J = 2.2$. Values of U, J, and y-axis energies are in eV. The labels indicating the high-symmetry points for the k-point path are taken from Ref. [64] for the body-centered cubic lattice.

described in Sec. III A, while the matrix $n^{(0)}_{m\sigma}$ is kept fixed to its LDA value. In Sec. IV B we show that even when $n^{(0)}_{m\sigma}$ is treated as a variational parameter, its change with respect to the LDA value is very small in the case of nonmagnetic iron. An immediate consequence of our fixing $n^{(0)}_{m\sigma}$ is that, as far as band structure is concerned, we do not need to worry about the explicit form of the double-counting energy $E_{\rm dc}$ for the Hamiltonian (56), which plays a role in determining the electronic structure only through the optimization of the

TABLE I. Variance of d-electron number operator, total spin and angular momentum for d orbitals, and band mass renormalization factors for e_g and t_{2g} orbitals for a LDA + G calculation without optimization of the natural density matrix for the atomic Hamiltonian displayed in Eq. (56). The value of κ is 0.2 eV. The values of U we used are listed in the first column, and those of J in the second. The band structure results corresponding to the first and to the last three rows of the table are plotted in Fig. 1. The last line of the table shows how orbital selectivity is more sensitive to Hund's exchange J than to Hubbard U.

U (eV)	J (eV)	$\langle(\Delta N)^2\rangle$	$\lvert S\rvert$	$\lvert L\rvert$	Z_{e_g}	$Z_{t_{2g}}$
0	0	2.30	0.89	3.22	1	1
2.5	1.2	1.37	1.00	3.27	0.94	0.96
5	1.2	1.10	1.03	3.29	0.90	0.93
10	1.2	0.82	1.04	3.31	0.82	0.87
10	2.2	0.78	1.25	3.05	0.72	0.82

natural density matrix. In Table I we show the band mass renormalization factors Z_{e_g} and $Z_{t_{2g}}$ for different values of Hubbard parameter U, whereas J is kept fixed along all rows of the table but the last one, where it is increased to 2.2 eV. Predictably, we cannot fully recover the non-Fermi liquid with e_g orbital-selective state obtained by Anisimov and co-workers [30] as a result of a DMFT, and, in fact, our Gutzwiller calculation shows just a minor localization of both e_g and t_{2g} orbitals, driven both by the Hubbard interaction U and by Hund's exchange J, the latter playing an important role in the orbital selectivity of the mass enhancement, as can be seen from the last row of Table I. It is at this stage not possible to clarify how much the weaker orbital selectivity resulting from our calculation could be due to the fact that our calculation is performed at zero temperature, as opposed to the finite-temperature approach by Anisimov and co-workers [30] or rather to the limitations of the Gutzwiller method. Indeed, because of the substantial hybridization between e_g and s

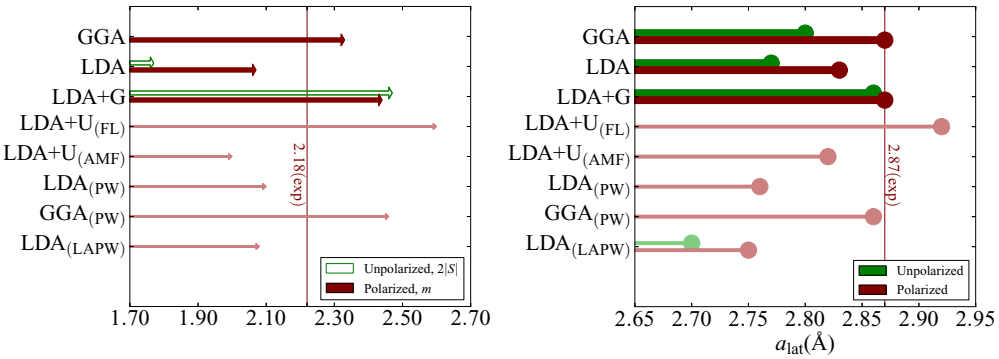

FIG. 2. (Color online) (Left) Magnetic moment $2|S|$ (for unpolarized calculations, open green arrows) and magnetization m (for polarized calculations, solid dark red arrows) within GGA, LDA, and LDA + G. The five thin pink arrows refer to previous calculations, the first four by Cococcioni and De Gironcoli [50] with the plane-wave (PW) pseudopotential QUANTUM ESPRESSO code, the LDA + U calculations being performed with the fully localized and the around-mean-field recipe for double counting, respectively. Our LDA results for the magnetic moment are in accord with the LDA linearized-augmented-plane-wave (LAPW) result by Wang *et al.* [25], which is shown by the last pink arrow. (Right) Lattice parameters listed for the same calculations. The LDA LAPW results by Wang report lattice parameters for unpolarized (pale green) and polarized (pink) iron which are both smaller than those we find. The SIESTA overestimation of lattice constant with respect to both LAPW and PW codes is most probably a result of the choice of the single-ζ basis set. The figures plotted in these graphs are listed also in Table III.

orbitals, ineffective close to the Γ point but appreciable in the rest of the Brillouin zone and especially close to the H point, a genuine localization of e_g electrons could not be directly unveiled by the GA, although indirect evidences can still be found, as we discuss later.

B. Ferromagnetic versus nonmagnetic iron: Correlation-induced enhancement of local magnetic moment

In order to address the magnetic properties of iron, we carried out spin-polarized and spin-unpolarized LDA, GGA, and LDA + G calculations, the latter now including optimization with respect to the natural orbital density matrix. In Tables II to VI we list the electronic structure data of bcc iron with optimized $n^{(0)}_{m\sigma}$. Reasonable values which we finally adopted for U and J are 2.5 and 1.2 eV, respectively. Both are close to, if only slightly larger than, those used by Anisimov and co-workers [30]. We observe—see second column of Table II—that the optimization of $n^{(0)}_{m\sigma}$ in the LDA + G unpolarized case causes only small changes in the matrix elements of the natural density matrix with respect to the LDA result. This confirms and provides an *a posteriori* justification of the results obtained in Sec. IV A and suggests that the natural density matrix is mainly determined by electrostatic balance, which is well captured by LDA and does not require a better account of correlation effects. The Gutzwiller parameters do provide the wave function with more flexibility, but do not seem to give any important feedback on the natural density matrix.

This feedback becomes instead important in the spin-polarized case, where it contributes to an increase relative to LDA of the total magnetization m and of the lattice parameter, as can be seen by comparing the values in the second column of Table III.

Within our Gutzwiller approach we can also compute the local spin moment $|S|$ of the d orbitals from the expectation value of S^2

$$S(S+1) = \mathrm{Tr}\{\hat{\Phi}^\dagger \hat{\mathbf{S}}\cdot\hat{\mathbf{S}}\,\hat{\Phi}\}. \tag{57}$$

Although fluctuating, in the ferromagnetic phase this moment is partly aligned with the z axis, thus contributing to the global magnetization order parameter m, which is instead computed from the Gutzwiller-renormalized density $n(\boldsymbol{r})$ as

$$m = \int d\boldsymbol{r}\,[n_\uparrow(\boldsymbol{r}) - n_\downarrow(\boldsymbol{r})]. \tag{58}$$

TABLE II. Orbital densities $n^{(0)}_\alpha$ and quasiparticle mass renormalization $m/m^* = R^2_{\alpha\alpha}$ for the different types of calculations performed, with $\alpha = e_g,t_{2g}$ and $e_g\uparrow, t_{2g}\uparrow, e_g\downarrow, t_{2g}\downarrow$ for unpolarized (unp.) and polarized (pol.) calculations, respectively. Optimization with respect to the natural density matrix is included.

	$n^{(0)}_\alpha$	m/m^*
LDA unp.	0.597,0.685	1,1
LDA pol.	0.920,0.823,0.303,0.515	1,1,1,1
LDA + G unp.	0.599,0.673	0.925,0.953
LDA + G pol.	0.936,0.880,0.277,0.457	0.969,0.967,0.984,0.984

TABLE III. Results for optimized lattice parameter a_{lat} (in Å), total magnetization m, magnetization m_d on d-type orbitals, and total spin $2|S|$ (in Bohr magnetons) on d orbitals. The last row shows the experimental values for lattice parameter and magnetization. Optimization with respect to the natural density matrix is included.

	a_{lat} (Å)	m	m_d	$2\|S\|$
GGA unp.	2.80			
GGA pol.	2.87	2.33		
LDA unp.	2.77			1.77
LDA pol.	2.83	2.066	2.14	2.61
LDA + G unp.	2.86			2.47
LDA + G pol.	2.87	2.44	2.58	3.04
Exp. [65]	2.87	2.22		

It is worth noting here that the increase in spin-polarized calculations of $2|S|$ from LDA to LDA + G is almost equal to the simultaneous increase in magnetization m (see Table III and Fig. 2), suggesting that the magnetization rise in LDA + G is mainly due to the larger local magnetic moment stabilized by correlations.

C. Energy balance in ferromagnetic vs nonmagnetic iron

Once spin polarization is allowed, the magnitude of the d-orbital local moment $|S|$ increases percentually less within LDA + G, roughly 20%, than within LDA, around 50%. In other words, the nonmagnetic, unpolarized LDA + G calculation already endows the iron atom with a Hund's rule local moment of the right magnitude, ready to align with all other atoms when given the possibility. The propensity towards magnetic order in LDA + G has a clear signature in the balance of the various contributions to the total energy. In Table IV we list the total energies of the various density functional calculations which we carried out, and in Table V (and in the corresponding Fig. 3) we list the energy differences between polarized and unpolarized calculations. In both tables the total energy is divided up into kinetic, electron-ion interaction plus electrostatic, and exchange-correlation contributions. In Table VI we indicate the error of LDA + G arising from the linearization (40) and (41) of the Hartree and exchange-correlation energies, respectively. We observe that these errors

TABLE IV. Total energy (eV/atom) for bcc iron computed with the different basis sets and functionals, divided in total energy, kinetic energy, atomic interaction plus electrostatic energy $E_{\mathrm{at+el}}$, and exchange-correlation energy. The quantity on the fourth column is equal to $E_{\mathrm{at+el}} = E_{\mathrm{ion}} + E_{\mathrm{ie}} + E_{\mathrm{H}} + E_{\mathrm{at}} - E_{\mathrm{dc}}$, where E_{at} is defined in Eq. (39) [with atomic Hamiltonian (10)], E_{dc} is defined in Eq. (13), and E_{ie} and E_{ion} are the electrostatic interaction energies between ions and electrons and between ions and ions.

	E_{tot}	E_{kin}	$E_{\mathrm{at+el}}$	E_{xc}
GGA unp.	−781.625	765.108	−1157.611	−389.121
GGA pol.	−782.235	769.901	−1161.603	−390.533
LDA unp.	−780.196	777.255	−1170.507	−386.943
LDA pol.	−780.567	777.947	−1171.205	−387.308
LDA + G unp.	−777.231	777.099	−1168.651	−385.682
LDA + G pol.	−777.499	774.182	−1165.568	−386.117

TABLE V. Energy differences (eV/atom) between the spin-polarized and unpolarized ground states of bcc Fe, taken from Table IV. By looking at the last two columns, one notices the opposite signs of kinetic and $E_{\mathrm{at+el}}$ gains when switching between the two ground states. The kinetic energy gain is connected with the increase of Gutzwiller band mass renormalization factors Z from spin-unpolarized to spin-polarized wave functions, as can be seen from Table II.

	δE_{tot}	δE_{kin}	$\delta E_{\mathrm{at+el}}$	δE_{xc}
GGA	− 0.61	4.79	− 3.992	− 1.412
LDA	− 0.37	0.692	− 0.698	− 0.365
LDA + G	− 0.27	− 2.92	3.083	− 0.44

are much smaller than the energy differences in Table V, which are therefore reliable.

Focusing on the last two rows in Table V, we can now explore the energy balance changes brought about by ferromagnetic order. While in LDA the onset of ferromagnetic long-range order is accompanied by a loss of kinetic energy overwhelmed by a gain of potential energy (the sum of electron-ion, Hartree, and exchange), the opposite actually occurs in LDA + G. While this specific aspect was not explored in previous calculations, elemental bcc iron emerges upon addition of electron correlation effects as a correlated material, where ferromagnetism appears as due, to a significant level, to the ordering of pre-existing moments driven by kinetic rather than potential energy gain. With the moderate and controlled improvement represented by Gutzwiller projection over LDA, the basic physical reason why the atomic magnetic moments of iron order ferromagnetically has thus turned completely around, from the direct intersite exchange upon which the itinerant picture portrays, to one that is closer to double exchange. The two e_g electrons per atom are essentially localized and lined up to spin 1. They couple via Hund's rule intra-atomic exchange to the remaining t_{2g} electrons, which, unlike the e_g, form a broad itinerant band. Due to that coupling, ferromagnetic interatomic alignment is required in order to allow the t_{2g} electrons (actually "holes") to propagate

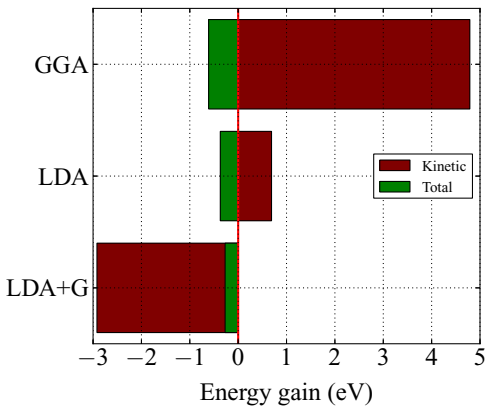

FIG. 3. (Color online) Total (green) and kinetic (red) energy gain (in eV per atom) of the spin-polarized relative to the spin-unpolarized phase of bcc iron. The values plotted are listed along the second and third columns of Table V.

TABLE VI. Estimated errors (in eV) due to the approximate expressions (40) and (41) for the Hartree and exchange-correlation energies respectively, listed for the spin-unpolarized and spin-polarized ground-state calculations. All errors are negligible with respect to the energy differences computed in Table V.

	ΔE_{H}	ΔE_{xc}
LDA + G unp.	0.0083	−0.0012
LDA + G pol.	0.0054	−0.0020

and thus reduce their kinetic energy [66,67], much as in double-exchange ferromagnetism in, e.g., manganites [68].

More in detail, the gain in kinetic energy is signaled by and consistent with the fact that the quasiparticle weights Z increase when the magnetization is allowed to appear as opposed to the nonmagnetic case, as can be seen in Table II. Thus, t_{2g} quasiparticles propagate better in the presence of ferromagnetic order, precisely as expected in the double-exchange mechanism. An even clearer theoretical evidence could, we believe, be extracted if one were able to perform a $\boldsymbol{k}$-resolved evaluation of quasiparticle weights, presently beyond our means. Double exchange is an intrinsically many-body effect which cannot be reproduced within theories that do not include band renormalization by electron-electron interactions. For this reason it cannot be uncovered by standard DFT calculations, whereas it would naturally occur as a consequence of a selective e_g electron localization, such as that suggested by LDA + DMFT [30,31] and confirmed here by LDA + G. The double-exchange process can only occur in the presence of long-lived on-site magnetic moments, which exist independently of their intersite ordering. Independent-electron, single-Slater-determinant based theories such as HF and LDA can only describe the birth of a magnetic moment through the simultaneous appearance of a net collective spin polarization, which provides the only element that permits a decrease of the electron-electron repulsive potential energy through the Pauli exclusion principle. The onset of magnetization, however, entails spatial restriction of electrons, with a resulting increase of kinetic energy, a characteristic feature of the itinerant Stoner-Wohlfarth picture [69]. We now find that this overall result of uncorrelated LDA is reversed upon inclusion of electronic correlations in iron using the Gutzwiller wave function. The Gutzwiller projection takes care of correctly reducing the large intra-atomic electron repulsion at the onset of a Hund's rule local moments, independently of collective ordering of local moments among themselves. The main lowering of potential energy is intra-atomic, thus not connected with interatomic ferromagnetic ordering. The collective ferromagnetic ordering successively permits the d-electron delocalization (mostly t_{2g} in Fe) which is otherwise impeded by incoherent spin polarizations of neighboring atoms. This gains some kinetic energy, sacrificing, in fact, some potential energy as also signaled by a slight decrease of on-site magnetic moments.

This overall finding, which also seems compatible with the LDA + DMFT results by Anisimov *et al.* [30,31], is sufficiently striking to call for strong attention, as well as for an independent future assessment of the accuracy of the correlations introduced by our Gutzwiller approach. In reality,

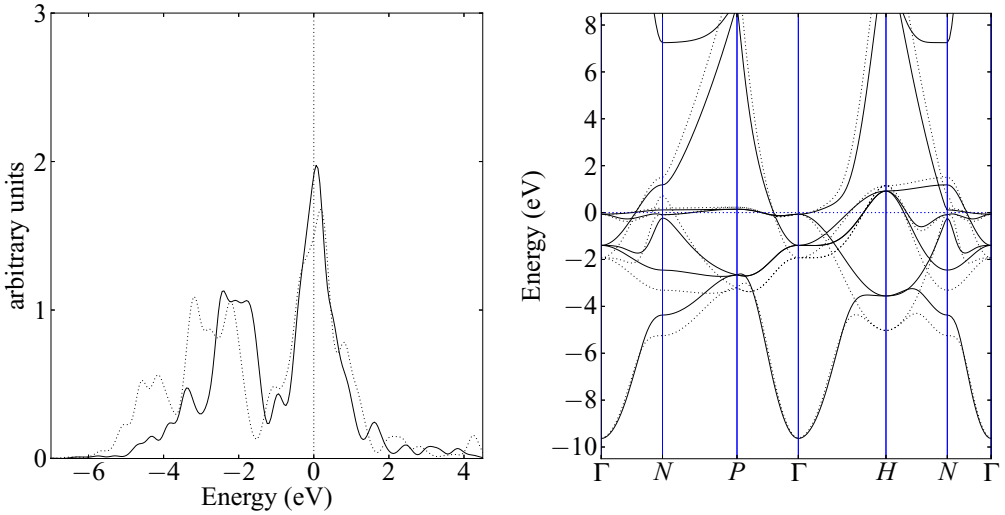

FIG. 4. (Color online) Comparison of projected density of states and band structure between spin-unpolarized LDA + G (solid lines) and LDA (dotted lines).

several properties of Fe around the Curie temperature can already be invoked in support of our results. Indeed, it is well known that magnetic splitting of electron bands survives well above T_C [70,71], suggestive of magnetic moments preexisting the onset of ferromagnetism. In addition, the Curie temperature does not diminish under pressure, as would be expected if magnetic order set in at the expense of the kinetic energy; rather, it slightly increases [72]. Finally, the electrical resistivity, ρ, drops quite sharply below T_C, and the slope $d\rho/dT$ versus temperature increases, actually almost doubles [71,73,74], indicating that the electrons move with more ease in the ferromagnet. In fact, all the above properties have been explained in the past by assuming a kind of two-fluid picture, with itinerant electrons scattering off the critical fluctuations of magnetic moments near their ordering temperature [75,76]. Evidently, such a two-fluid scenario is hard to conceive in the Stoner-Wohlfarth model, while it fits well with our findings.

D. Comparisons with LDA, GGA, LDA + U

The previous section presented our most important results. Before closing, we discuss some other general results of the LDA + G calculation in comparison with those of different approximations. Even without expecting improvements over previous highly accurate calculations, such as the spin-polarized GGA (see, e.g., Ref. [25]), because of our limited basis set, it is instructive to compare the band structures and density of states obtained within LDA, LDA + G, and GGA, shown in Figs. 4–7, and estimated lattice parameters, magnetization, and total magnetic moment, see Fig. 2.

The SIESTA GGA prediction for the iron lattice parameter is 2.87 Å, in good agreement with the experimental value, while its magnetic moment is slightly overestimated (2.33 vs 2.22 Bohr magnetons; see Ref. [65]). We note that LDA + G corrects, without a need for gradient terms, the lattice parameter underestimation which is a well-known flaw of LDA. LDA + G also increases the total magnetic moment from

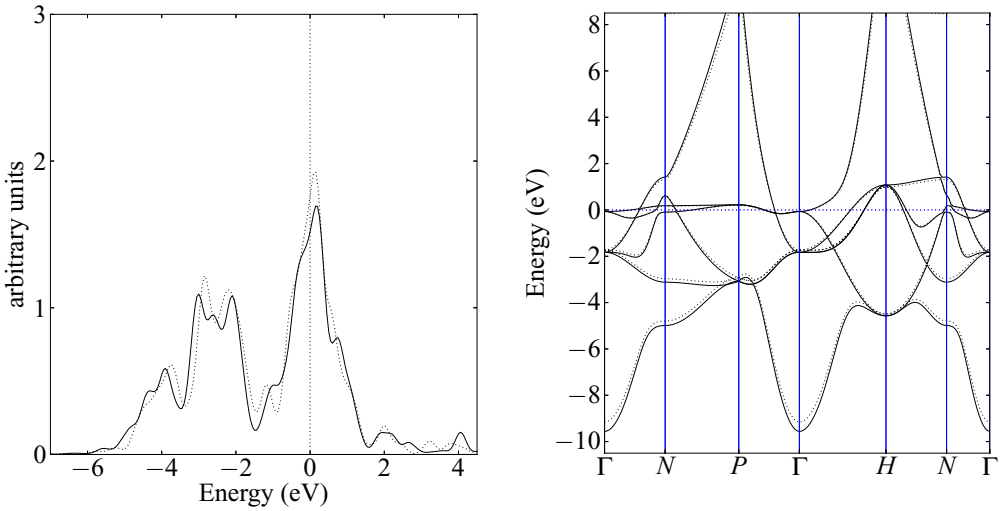

FIG. 5. (Color online) Comparison of projected density of states and band structure between spin-unpolarized LDA + G (solid lines) and GGA (dotted lines).

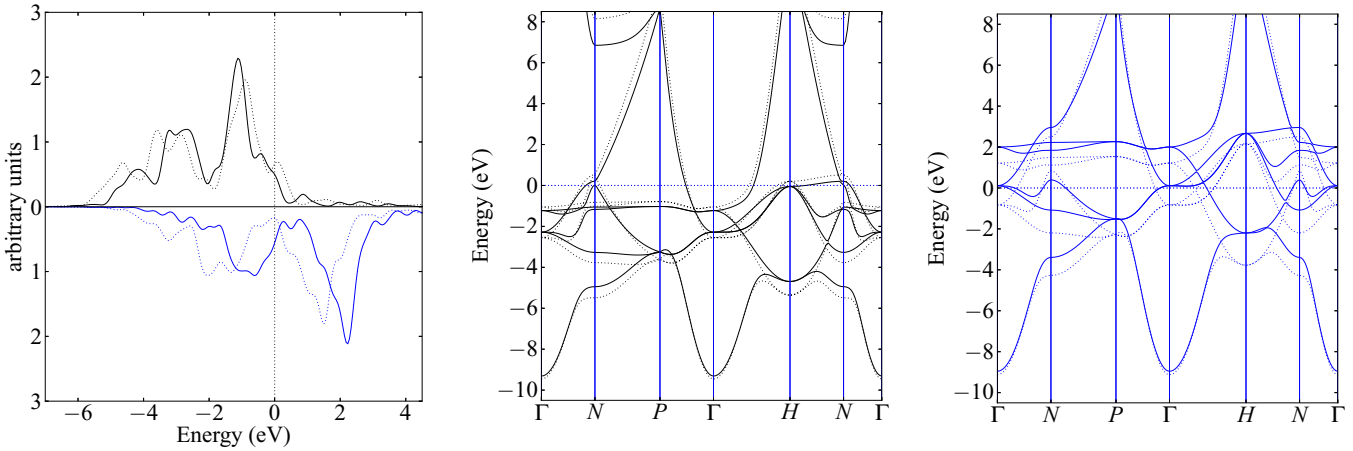

FIG. 6. (Color online) Comparison of projected density of states and band structure between spin-polarized LDA + G (solid lines) and LDA (dotted lines). The line colors blue and black refer to minority and majority components, respectively.

the underestimated LDA value to a slightly overestimated one, now larger than the GGA result (see again Fig. 2). Comparing the polarized band structures, we note an upward shift of the minority band in LDA + G with respect to GGA, consistent with the larger magnetization obtained by the former, although the shapes are quite similar. In particular, the minority band at Γ within LDA + G lies above the Fermi energy, while it is below in GGA and in experiments (see Fig. 8) [77–79]. The detailed band behavior near Γ is notoriously delicate, as recently discussed in Ref. [77], and depends crucially on all parameters that contribute to determine the precise value of magnetization, not least the uncertainty in the expression of the double-counting term. Previous LDA + U calculations of iron [43,50] indeed pointed out the differences arising by using an around-mean-field instead of a fully localized expression for the double-counting energy, a question that would be worth further investigation [80].

V. FINAL REMARKS

We presented here the step-by-step implementation protocol of a simplified density-self-consistent scheme integrating the standard local density functional formalism of Kohn and Sham DFT with that implied by Gutzwiller wave-function corrections. Other applications of the Gutzwiller method to realistic electronic structure calculations have recently appeared. Bünemann, Weber, and Gebhard [81–83] implemented a non-self-consistent Gutzwiller approach to electronic structure calculations, where a tight-binding model was set up from effective hopping parameters computed through a Kohn-Sham density functional calculation, and afterwards solved within the multiband GA. An approach where both density and Gutzwiller parameters are optimized self-consistently was proposed in Refs. [17] and [13] and applied to several case studies [11,15], including Fe [12]. This method is in principle similar to ours, with the difference that it does not include the possibility of using a projector with nonzero off-diagonal matrix elements, which is instead a natural feature of our mixed-basis parametrization with $\hat{\Phi}$ operators. More recently, a fully unrestricted and density self-consistent Gutzwiller + LDA approach has been proposed [16] and applied to the γ-α isostructural transition of Ce [18]. This method is in its formulation equivalent to ours, though different in the implementation.

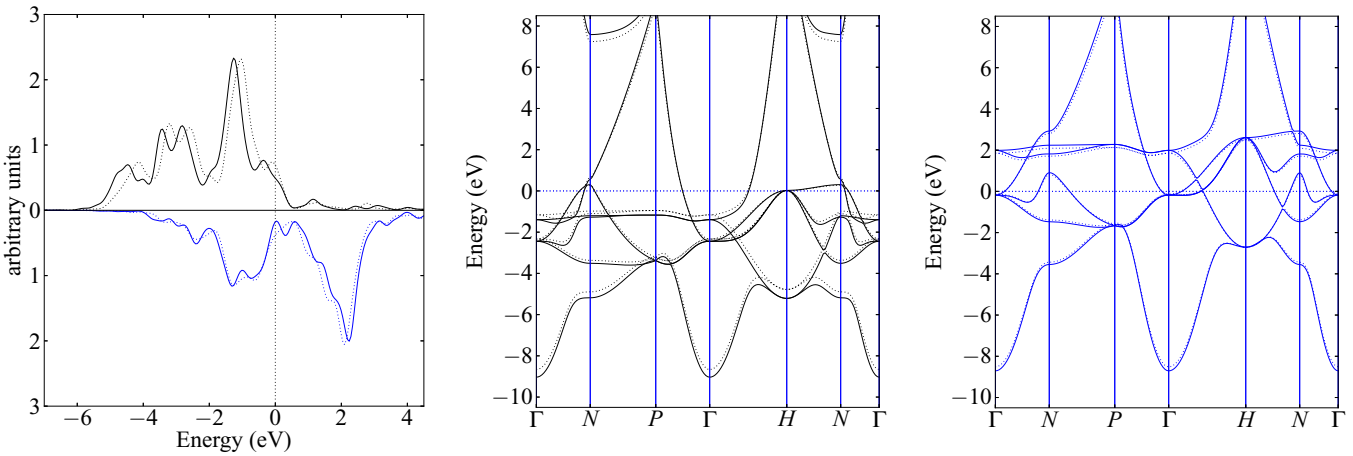

FIG. 7. (Color online) Comparison of projected density of states and band structure between spin-polarized LDA + G (solid lines) and GGA (dotted lines). The line colors blue and black refer to minority and majority components, respectively.

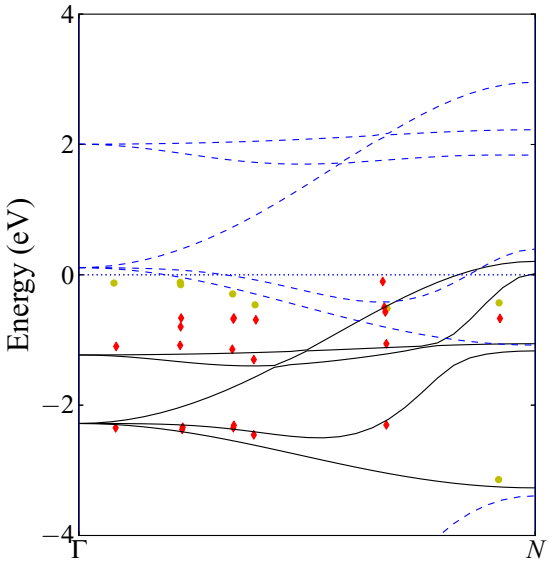

FIG. 8. (Color online) Comparison of band structure of spin-polarized iron within LDA + G (black lines for majority, blue dashed lines for minority spin) with photoemission data taken from Ref. [79]. Red diamonds refer to majority spin and yellow circles refer to minority spin.

As an important and basic application, we applied the resulting LDA + G method to the electronic structure of bcc Fe, where important open questions about the role of correlations still remain, including the possibility of an orbital-selective localization of e_g electrons; see Ref. [30] and references therein. Although we did not find an actual orbitally selective localization of electrons, our results confirm that the magnetism of iron is, at least partially, driven by a double-exchange mechanism, caused by stronger localization of e_g states relative to t_{2g} ones, a typically many-body phenomenon not described by conventional DFT. The double exchange mechanism would, of course, also arise as a direct consequence of a selective e_g localization. This dual, itinerant and localized, character of ferromagnetism in iron has been often invoked to explain the persistence of magnetic excitations well above the Curie temperature [70] (see, e.g., Refs. [76] and [84]), which clearly cannot be captured by the mean-field scenario of spin-polarized LDA. LDA + G instead provides a unified framework where both itinerant and localized characters can be described within the same electronic structure calculation. We note that a gain of kinetic energy has been proposed earlier as the source of ferromagnetic ordering by Hirsch, who demonstrated it in detail in the case of EuB_6 [34].

The Gutzwiller approach predicts an enhancement of local moments, already at the unpolarized LDA level. The spin-polarized calculation separately provides the energy gain caused by interatomic magnetic alignment and ordering. The two phenomena, onset of magnetic moment and ordering, which come by necessity together and are treated on the same footing within simple LDA, local spin density approximation (LSDA), and LDA + U, are correctly very distinct within LDA + G. Identifying and pursuing experimental evidence for the double exchange mechanism in the ferromagnetic ordering of Fe is, of course, a very relevant question. Most of it is implicit in the well-known survival of the local moment above the Curie temperature [70] and in the lack of pressure decrease of the Curie temperature itself [72]. As for what concerns our method, even at zero temperature there is ample room for improvement. Besides a desirable enlargement of the basis, the present calculations of the electronic structure of Fe through LDA + G implemented in the SIESTA code could be further perfected. For example, and first of all, this could be done with the inclusion of two separate hopping renormalization factors on each e_g and t_{2g} multiplet of a double-ζ basis set, through which we would be able to better account for the effects of Hubbard-U and exchange parameter J on electron localization. The slightly excessive magnetic moment we found can most likely be corrected through a better choice for the Hubbard-U and by an improved evaluation of double-counting energy. In spite of the great number of parameters contained in $\hat{\Phi}$, the Lanczos-enhanced LM algorithm we implemented here for the minimization of the energy with respect to Gutzwiller parameters is stable and fast and can be easily parallelized to deal with more complex systems such as crystals having more than one atom per unit cell as transition-metal compounds.

ACKNOWLEDGMENTS

We thank Nicola Lanatà for useful suggestions and discussions. G.B. acknowledges Gia-Wei Chen for useful remarks on the manuscript. E.T. thanks Jorge E. Hirsch, who kindly pointed out his earlier work on kinetic energy gain as a source of ferromagnetism. This project was completed during the tenure in Trieste of Contract No. PRIN/COFIN 2010LLKJBX 004, EU-Japan Project No. LEMSUPER, Grant Agreement No. 283214, and ERC Advanced Grant No. 320796 MODPHYSFRICT. We also acknowledge financial support by the European Union, Seventh Framework Programme, under the project GO FAST, Grant Agreement No. 280555.

APPENDIX A: IMPOSING SYMMETRIES ON THE GUTZWILLER PROJECTOR

The easiest basis in which to define the Gutzwiller projector is the basis of Slater determinants of single-particle wave functions, which we indicate in the text as the basis of electronic configurations (BC). A sample N-particle configuration on d orbitals is, for instance, the five-electron, maximum-spin configuration, which in second quantized form reads

$$\left(\prod_{m=-2}^{2} c^{\dagger}_{m\uparrow}\right)|0\rangle. \tag{A1}$$

If we wish to write the most general projector in the BC, the number of parameters we need is, in principle, equal to $2^{2(2l+1)} \times 2^{2(2l+1)}$, where $2^{2(2l+1)}$ is the size of the many-body Hilbert space for multiplet of orbitals of angular momentum l. This is a huge number, which is hardly possible to treat with numerical optimization already when $l = 4$ or 5. In order to lower the amount of parameters that build up a Gutzwiller projector, we need to switch from this type of configuration basis, whose states are identified by single-particle quantum numbers as single-particle spin σ and magnetic quantum

number m, to a basis of multiparticle quantum numbers that are good quantum numbers of the problem we are studying, which are, in the case of a system with full rotational invariance, the total spin S^2, the total angular momentum L^2, and the total spin and angular momentum magnetic quantum numbers S_z and L_z, respectively. We refer to this basis of many-body states labeled by good quantum numbers of the problem as the many-body symmetric basis (MBSB). In the case of paramagnetic iron, the orbital rotational symmetry is broken by the cubic crystal field, resulting in a different set of conserved orbital quantum numbers, corresponding to the irreducible representations of the cubic group. In the case of spin-polarized iron, also the spin rotational invariance is broken in favor of a lower spin easy-axis symmetry, where only S_z remains a good quantum number.

1. Spin rotational symmetry

It is well known (see, for instance, Ref. [85]) that the eigenstates of the total spin operator square S^2 on the basis of a set of N spins can be written in terms of Young tableaux. This is possible because of the isomorphism between the group $SU(N)$ and the irreducible representations of the permutation group, which are represented by Young tableaux. A general tableau provides a rule for the symmetrization-antisymmetrization with respect to particle exchange of a Slater determinant with a given number of electrons in a given orbital and spin configuration. Each box of a tableau corresponds to a particular filled single-particle orbital state, containing either a spin-up ($\uparrow$) or a spin-down ($\downarrow$) electron. The orbitals belonging to the same row of a tableau must be symmetrized, while those belonging to different rows must be antisymmetrized. The many-body wave function produced by this symmetrization-antisymmetrization recipe turns out to be an eigenstate of both $\mathbf{S}\cdot\mathbf{S}$ and S_z. The eigenvalue of S_z can be obtained by summing the spins in each box of the tableau, while the eigenvalue of $\mathbf{S}\cdot\mathbf{S}$ corresponds to the tableau shape. For instance, the state with maximum S_z component on d orbitals is built from the totally symmetric tableau,

$$\boxed{\uparrow}\boxed{\uparrow}\boxed{\uparrow}\boxed{\uparrow}\boxed{\uparrow}, \tag{A2}$$

which corresponds to $S = 5/2$. This particular state is a single Slater determinant, already belonging to the basis of configurations. The row-wise antisymmetrization rule of a tableau automatically imposes the Pauli principle on the wave function, so that only wave functions obtained from one-column tableaux, or two-column tableaux with opposite spins on each column, are nonzero. For instance, the two-particle singlet state has a simple representation in terms of the totally antisymmetric two-particle tableau,

$$\begin{array}{|c|}\hline\uparrow\\\hline\downarrow\\\hline\end{array}, \tag{A3}$$

applied to a couple of electrons with opposite spin. By application of raising and lowering operators S^+ and S^- on a many-body wave function, one obtains another wave function which is generated by a tableau of the same shape. Every wave function with fixed values of S and S_z has an additional degeneracy which can be computed from the shape of the generating tableau, according to some simple rules [85].

2. Implementation of crystal point symmetry

In order to provide a classification of many-body wave functions according to point group quantum numbers, it is necessary to label them with angular momentum quantum numbers.

a. Building eigenstates of angular momentum

Thanks to Young tableaux we are able to label states with the quantum numbers $\{N, S^2, S_z, L_z\}$. For each of these sets of quantum numbers, there are several states with different values of the square modulus $L(L+1)$ of total angular momentum. If the BC of our problem is already built from single-particle eigenstates of $\mathbf{L}\cdot\mathbf{L}$ and L_z, as for instance the $3d$ orbitals of a transition metal ($l = 2$), it is very easy to build the angular momentum raising operator explicitly,

$$L^+ = \sum_{m=-l}^{l-1} \sqrt{l(l+1) - m(m+1)}\, c^\dagger_{m+1} c_m. \tag{A4}$$

From $\mathbf{L}\cdot\mathbf{L} = L^+L^- + L_z\left(L_z - 1\right)$ we can build the operator $\mathbf{L}\cdot\mathbf{L}$, which will be block diagonal in every subspace with fixed $\{N, S^2, S_z, L_z\}$. The diagonalization of every block gives the desired set of states, labeled by $\{N, S^2, S_z, L_z\}$. For large many-body spaces, as for instance the one built from d-electrons of a transition metal, another index θ might be needed in order to distinguish between different states having the same set of quantum numbers listed above.

3. Building eigenstates of point group symmetry operators

Provided that a set of many-body eigenstates of spin and angular momentum operators has been given, it is easy to break the rotational symmetry of the MBSB in favor of some lower crystal symmetry when necessary. In this section we treat the case of cubic symmetry, which is the case of iron. The ingredients we need for this purpose are just the following:

(1) the 3×3 matrix representation $G(g)_{ij}$ of the action of each element g of the cubic group on a three-dimensional vector $\boldsymbol{r}$;

(2) the character table of the group (for the cubic group it is shown in Table VII);

(3) the $\boldsymbol{r}$-space representation in spherical coordinates of an external potential with the symmetry of the group; an

TABLE VII. Character table of the cubic group. The first row lists all the group classes along with the number of symmetry operations they contain. The following rows list the irreducible representations and their character on each symmetry class. From Ref. [86].

	E	$8C_3$	$3C_2(C_4^2)$	$6C_2$	$6C_4$
A_1	1	1	1	1	1
A_2	1	1	1	−1	−1
E	2	−1	2	0	0
T_1	3	0	−1	−1	1
T_2	3	0	−1	1	−1

example for a potential with cubic symmetry is

$$v[\hat{\boldsymbol{r}}(\theta,\phi)] = \cos(\theta)^4 + \tfrac{1}{4}[3+\cos(4\phi)]\sin(\theta)^4, \qquad \text{(A5)}$$

where $\hat{\boldsymbol{r}}$ is the radial unit vector.

Once these three ingredients are at hand, we proceed as follows.

(i) For each set of spherical harmonics $Y_{L,m}(\theta,\phi)$ with given L, we compute (by means of the algorithm of Gimbutas *et al.* [87]) and diagonalize the matrix

$$C^{(L)}_{m,m'} = \int Y^*_{L,m}(\hat{\boldsymbol{r}})v(\hat{\boldsymbol{r}})Y_{L,m'}(\hat{\boldsymbol{r}})\,d\Omega. \qquad \text{(A6)}$$

(ii) For each set of spherical harmonics with given l and for each group element g, we calculate the matrix elements

$$M(g)^L_{m,m'} = \int Y^*_{L,m}(\hat{\boldsymbol{r}})Y_{L,m'}(G(g)^{-1}\hat{\boldsymbol{r}})\,d\Omega. \qquad \text{(A7)}$$

(iii) For each eigenvalue ε of the matrix $C^{(L)}$, and for all eigenvectors $c^{\varepsilon,L,i}$ relative to this eigenvalue, we compute the character

$$\chi(\mathcal{C},L,\varepsilon) = \sum_i \sum_j c^{\varepsilon,L,i}_j M(g\in\mathcal{C})^L_{jk} c^{\varepsilon,L,i}_k \qquad \text{(A8)}$$

relative to the class $\mathcal{C}$. The value of the character enables us to assign the correct label of irreducible representation $\mathcal{I}$ to the eigenvectors $c^{\varepsilon,L,i}$.

The matrices $U^{(L)}_{ij} = c^{\varepsilon,L,i}_j$ are the unitary matrices we need to apply to every block of many-body basis states with a given value of L in order to switch from a basis labeled with $\{N,S^2,S_z,L^2,L_z\}$ to a basis indicated by $\{N,S^2,S_z,L^2,\mathcal{I},\iota\}$, where ι labels the states within the same irreducible representation $\mathcal{I}$ (the quantum number L is still used to label states since each irreducible representation of the cubic group comes from a definite representation of the rotation group $O(3)$. However, in the case of cubic symmetry L is no longer a conserved quantum number, and the ground-state of the Hamiltonian will not necessarily have a definite L).

APPENDIX B: BUILDING THE MOST GENERAL GUTZWILLER PARAMETER MATRIX

In this section we show how to parametrize the matrix $\hat{\Phi}$of Gutzwiller parameters in the case of full spin and orbital rotational symmetry. The procedure is similar in the case of cubic symmetry.

We can easily construct the most general Gutzwiller parameter matrix $\hat{\Phi}$ commuting with the operators $\hat{S}^2$, $\hat{L}^2$, $\hat{S}_{x,y,z}$, and $\hat{L}_{x,y,z}$ by the following procedure.

(1) Operatively, we find the quantum numbers that uniquely identify the irreducible representation of the symmetry group, in this case spin and spatial rotations $SU(2)\times O(3)$. These quantum numbers are $\boldsymbol{\alpha} = \{N,S,L\}$. The same representation can appear multiple times, so we add another quantum number θ to distinguish between equivalent representations. Each irreducible representation has a degeneracy $n_{\{\boldsymbol{\alpha},\theta\}} = L(L+1)\times S(S+1)$; we distinguish between states that are a basis for the same irreducible representation $\{\boldsymbol{\alpha},\theta\} = \{N,S,L,\theta\}$ through the index $\iota = \iota(\boldsymbol{\alpha}\theta)$. In the case of spin and rotational symmetry ι lists all the eigenstates of $\hat{S}_z$ and $\hat{L}_z$ within the same S and L.

(2) With the previous definitions, the matrix elements of $\hat{\Phi}$ are labeled

$$\Phi_{\boldsymbol{\alpha}\theta\iota,\boldsymbol{\beta}\theta'\iota'} = \delta_{\boldsymbol{\alpha}\boldsymbol{\beta}}\delta_{\iota\iota'}\phi^{\boldsymbol{\alpha}}_{\theta\theta'}, \qquad \text{(B1)}$$

where $\phi^{\boldsymbol{\alpha}}_{\theta\theta'}$ is a reduced matrix element. The labels $\boldsymbol{\alpha}\theta\iota$ and $\boldsymbol{\beta}\theta'\iota'$ identify univocally one state of the MBSB, so that our parametrization of $\hat{\Phi}$ is complete.

The same recipe holds when the spatial symmetry is, for example, the crystal cubic symmetry. In this case, $\boldsymbol{\alpha} = \{N,S,\mathcal{I}\}$.

The result expressed by Eq. (B1) comes directly from Schur's lemma, which states that a matrix commuting all the matrices of an irreducible representation of a group $\mathcal{G}$ must be a multiple of identity. The matrix $\Phi_{\boldsymbol{\alpha}\theta\iota,\boldsymbol{\beta}\theta'\iota'}$ must be nonzero only for $\boldsymbol{\alpha} = \boldsymbol{\beta}$ since, if $\hat{G}$ is a generator of the group and $\varepsilon_{\boldsymbol{\alpha}}$ its eigenvalue with respect to any basis vector belonging to irreducible representation α, the commutation relations $[\hat{\Phi},\hat{G}] = 0$ imply that

$$\hat{G}\hat{\Phi}|\boldsymbol{\alpha}\,\rangle = \hat{\Phi}\hat{G}|\Psi_{\boldsymbol{\alpha}}\,\rangle = \varepsilon_{\boldsymbol{\alpha}}\hat{\Phi}|\Psi_{\boldsymbol{\alpha}}\rangle \qquad \text{(B2)}$$

and that $\hat{\Phi}|\boldsymbol{\alpha}\rangle$ must be a vector with the same quantum numbers $\boldsymbol{\alpha}$.

Again from the condition of zero commutator, we have that $\Phi_{\boldsymbol{\alpha}\theta\iota,\boldsymbol{\alpha}\theta'\iota'}$, seen as a matrix in the indices $\iota\iota'$ with fixed $\theta = \theta'$, must commute with all the matrices of irreducible representation $\boldsymbol{\alpha}$, and by Schur's lemma it must be a multiple of the identity matrix. For $\theta \neq \theta'$ the same statement does not hold, since the representations are distinct.

However, their equivalence implies that the matrices of the first are related to the matrices of the second through a unitary transformation. We can choose this transformation to be the identity, and this enables us to draw for $\theta \neq \theta'$ the same conclusions as for $\theta = \theta'$, so that $\Phi_{\boldsymbol{\alpha}\theta\iota,\boldsymbol{\alpha}\theta'\iota'}$ is diagonal in $\iota\iota'$ irrespectively of θ and θ'.

1. Symmetry reduction of parameter space

The procedure explained in the previous paragraphs makes it possible to considerably reduce the number of parameters for the Gutzwiller projector, so that its numerical optimization becomes not only computationally feasible, but also reasonably cheap. In Table VIII we list the sizes of local many-body irreducible representations and the number of independent Gutzwiller parameters compatible with a few different spin and point symmetries.

TABLE VIII. Number of many-body irreducible representations generated by d electrons and size of Gutzwiller parameter space for different types of spin (first column) and point (second column) symmetries. The symbol $U(1)$ refers to axial spin symmetry, $SU(2)$ to full rotational symmetry, $O(3)$ to full spatial rotational symmetry.

Spin symmetry	Point symmetry	# Hilbert	# Φ
$SU(2)$	$O(3)$	78	112
$U(1)$	$O(3)$	176	336
$SU(2)$	Cubic	197	873
$U(1)$	Cubic	428	2716

APPENDIX C: SPARSE-CONSTRAINED LEVENBERG MARQUARDT ALGORITHM

This algorithm performs the minimization of the Gutzwiller variational energy Eq. (50) with respect to the matrix elements of $\hat{\Phi}$. The details of the conventional constrained Levenberg-Marquardt (LM) algorithm are well explained by Fletcher [60], who suggests the multiplier penalty functional method (also known as augmented Lagrangian method) as a way to impose constraints.

Levenberg-Marquardt algorithm with Lanczos approximation for the Hessian

Depending on the quantity of single-particle orbitals involved in the definition of the Gutzwiller parameter matrix, the number of parameters x_i in the block-diagonal matrix $\Phi_{\alpha\beta}$ can be very large, which makes it computationally very expensive to compute the inverse Hessian matrix $\boldsymbol{h}^{-1}$, which is needed in the LM algorithm in order to find the descent direction $\boldsymbol{\delta}$, from the equation

$$\sum_j h_{ij}\delta_j = -g_i, \tag{C1}$$

where $\boldsymbol{g}$ is the gradient of Gutzwiller variational energy with respect to Gutzwiller parameters. Provided that $\boldsymbol{h}$ is positive-definite (and it can be modified to be so if necessary [60]), it can be convenient to solve Eq. (C1) within a smaller parameter space, defined by taking several Lanczos steps through the Hessian matrix $\boldsymbol{h}$. Also the memory storage of the algorithm can take great advantage of this possibility, since the definition of the Lanczos basis does not have as a requirement the knowledge of the full matrix h_{ij}, but only the knowledge of products $h_{ij}x_j$. Keeping in memory the full Hessian matrix is possible only for a small number of parameters, while it implies a considerable slow down of simulations in the case of a five-band Gutzwiller projector like the one we need for dealing with transition metals. Whenever we choose the starting Lanczos vector, we need to remember that finding an accurate solution for Eq. (C1) requires the solution vector $\boldsymbol{\delta}$ to have a nonzero component on the first vector $\boldsymbol{x}$ of the Lanczos chain. It can be shown that, provided $\boldsymbol{h}$ is positive definite, the choice of the gradient $\boldsymbol{g}$ as a starting vector ensures that $\boldsymbol{\delta}$ has nonzero components on the first three vectors of the Lanczos chain. Indeed, from the positive definiteness of $\boldsymbol{h}$ we get that

$$\sum_{ij} \delta_i^* h_{ij}\delta_j > 0, \tag{C2}$$

but since $\boldsymbol{\delta}$ must be such that $\sum_j h_{ij}\delta_j = -g_i$ [see Eq. (C1)], we have that

$$g_i^*\delta_i < 0, \tag{C3}$$

so that $\boldsymbol{g}$ has a nonzero component on $\boldsymbol{\delta}$. However, we can say more than this, namely that there is a nonzero component of $\boldsymbol{\delta}$ also on $\boldsymbol{hg}$, since

$$\sum_{ij} \delta_j^* h_{ij} g_i = -\sum_{ij} (g_i^* h_{ij}\delta_j)^* = -\sum_j g_j g_j^* < 0, \tag{C4}$$

provided that the gradient is finite. Finally, there is a nonzero component of $\boldsymbol{\delta}$ also on $\boldsymbol{h}^2\boldsymbol{g}$, again due to the positive definiteness of the Hessian,

$$\begin{aligned}\sum_{ij} \delta_i^* [h^2]_{ij} g_j &= \sum_{ij} \{g_i^* [h^2]_{ij}\delta_j\}^* \\ &= -\sum_i \{g_i^* h_{ij} g_j\}^* < 0.\end{aligned} \tag{C5}$$

This means that three Lanczos steps will certainly improve a steepest descent problem. Any further step will further refine the approximation to the correct descent direction $\boldsymbol{\delta}$. With the choice of the gradient as starting vector for the Lanczos chain, this minimization algorithm reduces to a constrained steepest descent in the limit of a single-vector Lanczos chain.

[1] N. F. Mott, Proc. Phys. Soc. A **62**, 416 (1949).
[2] N. F. Mott, *Metal Insulator Transition* (Taylor & Francis, London, 1990).
[3] W. M. C. Foulkes, L. Mitas, R. J. Needs, and G. Rajagopal, Rev. Mod. Phys. **73**, 33 (2001).
[4] U. Schollwöck, Rev. Mod. Phys. **77**, 259 (2005).
[5] A. Georges, G. Kotliar, W. Krauth, and M. J. Rozenberg, Rev. Mod. Phys. **68**, 13 (1996).
[6] M. C. Gutzwiller, Phys. Rev. **134**, A923 (1964).
[7] M. C. Gutzwiller, Phys. Rev. **137**, A1726 (1965).
[8] J. Bünemann, W. Weber, and F. Gebhard, Phys. Rev. B **57**, 6896 (1998).
[9] P. Fazekas, *Lecture Notes on Electron Correlation and Magnetism* (World Scientific, Singapore, 1999).
[10] W. F. Brinkman and T. M. Rice, Phys. Rev. B **2**, 4302 (1970).
[11] Y. X. Yao, C. Z. Wang, and K. M. Ho, Int. J. Quantum Chem. **112**, 240 (2012).
[12] X. Y. Deng, X. Dai, and Z. Fang, Europhys. Lett. **83**, 37008 (2008).
[13] X. Y. Deng, L. Wang, X. Dai, and Z. Fang, Phys. Rev. B **79**, 075114 (2009).
[14] T. Schickling, F. Gebhard, J. Bünemann, L. Boeri, O. K. Andersen, and W. Weber, Phys. Rev. Lett. **108**, 036406 (2012).
[15] G. T. Wang, Y. Qian, G. Xu, X. Dai, and Z. Fang, Phys. Rev. Lett. **104**, 047002 (2010).
[16] N. Lanatà, H. U. R. Strand, X. Dai, and B. Hellsing, Phys. Rev. B **85**, 035133 (2012).
[17] K. M. Ho, J. Schmalian, and C. Z. Wang, Phys. Rev. B **77**, 073101 (2008).
[18] N. Lanatà, Y.-X. Yao, C.-Z. Wang, K.-M. Ho, J. Schmalian, K. Haule, and G. Kotliar, Phys. Rev. Lett. **111**, 196801 (2013).
[19] M.-F. Tian, X. Y. Deng, Z. Fang, and X. Dai, Phys. Rev. B **84**, 205124 (2011).
[20] N. Lanatà, H. U. R. Strand, G. Giovannetti, B. Hellsing, L. de' Medici, and M. Capone, Phys. Rev. B **87**, 045122 (2013).
[21] D. J. Singh, W. E. Pickett, and H. Krakauer, Phys. Rev. B **43**, 11628 (1991).
[22] L. Stixrude, R. E. Cohen, and D. J. Singh, Phys. Rev. B **50**, 6442 (1994).

[23] A. Dal Corso and S. de Gironcoli, Phys. Rev. B **62**, 273 (2000).
[24] S. Y. Savrasov, Phys. Rev. Lett. **81**, 2570 (1998).
[25] C. S. Wang, B. M. Klein, and H. Krakauer, Phys. Rev. Lett. **54**, 1852 (1985).
[26] H. C. Herper, E. Hoffmann, and P. Entel, Phys. Rev. B **60**, 3839 (1999).
[27] A. J. Hatt, B. C. Melot, and S. Narasimhan, Phys. Rev. B **82**, 134418 (2010).
[28] J. B. Goodenough, Phys. Rev. **120**, 67 (1960).
[29] D. Vollhardt, N. Blümer, K. Held, and M. Kollar, in *Band-Ferromagnetism*, edited by K. Baberschke, M. Donath, and N. W., Lecture Notes in Physics Vol. 580 (Springer, Heidelberg, 2001), pp. 191–207.
[30] A. A. Katanin, A. I. Poteryaev, A. V. Efremov, A. O. Shorikov, S. L. Skornyakov, M. A. Korotin, and V. I. Anisimov, Phys. Rev. B **81**, 045117 (2010).
[31] A. S. Belozerov, I. Leonov, and V. I. Anisimov, Phys. Rev. B **87**, 125138 (2013).
[32] G. Stollhoff and P. Thalmeier, Z. Phys. B: Condens. Matter **43**, 13 (1981).
[33] M. B. Stearns, Phys. Rev. B **8**, 4383 (1973).
[34] J. E. Hirsch, Phys. Rev. B **59**, 436 (1999).
[35] V. I. Anisimov, J. Zaanen, and O. K. Andersen, Phys. Rev. B **44**, 943 (1991).
[36] V. I. Anisimov, F. Aryasetiawan, and A. I. Lichtenstein, J. Phys.: Condens. Matter **9**, 767 (1997).
[37] M. Levy, Proc. Natl. Acad. Sci. USA **76**, 6062 (1979).
[38] M. Levy, Phys. Rev. A **26**, 1200 (1982).
[39] E. Lieb, Int. J. Quantum Chem. **24**, 243 (1983).
[40] P. Hohenberg and W. Kohn, Phys. Rev. **136**, B864 (1964).
[41] T. Körzdörfer, J. Chem. Phys. **134**, 094111 (2011).
[42] A. I. Liechtenstein, V. I. Anisimov, and J. Zaanen, Phys. Rev. B **52**, R5467 (1995).
[43] A. G. Petukhov, I. I. Mazin, L. Chioncel, and A. I. Lichtenstein, Phys. Rev. B **67**, 153106 (2003).
[44] V. I. Anisimov and O. Gunnarsson, Phys. Rev. B **43**, 7570 (1991).
[45] C. Corliss and J. Sugar, J. Phys. Chem. Ref. Data **11**, 135 (1982).
[46] R. D. Cowan, *Theory of Atomic Structure and Spectra* (University of California Press, Oakland, 1981).
[47] S. L. Dudarev, G. A. Botton, S. Y. Savrasov, C. J. Humphreys, and A. P. Sutton, Phys. Rev. B **57**, 1505 (1998).
[48] V. I. Anisimov, I. V. Solovyev, M. A. Korotin, M. T. Czyzyk, and G. A. Sawatzky, Phys. Rev. B **48**, 16929 (1993).
[49] M. T. Czyzyk and G. A. Sawatzky, Phys. Rev. B **49**, 14211 (1994).
[50] M. Cococcioni and S. de Gironcoli, Phys. Rev. B **71**, 035105 (2005).
[51] A. Floris, S. de Gironcoli, E. K. U. Gross, and M. Cococcioni, Phys. Rev. B **84**, 161102 (2011).
[52] H. J. Kulik, M. Cococcioni, D. A. Scherlis, and N. Marzari, Phys. Rev. Lett. **97**, 103001 (2006).
[53] K. Haule and G. Kotliar, New J. Phys. **11**, 025021 (2009).
[54] Z. P. Yin, K. Haule, and G. Kotliar, Nat. Mater. Res. Bull. **10**, 932 (2011).
[55] Z. P. Yin, K. Haule, and G. Kotliar, Nat. Phys. **7**, 294 (2011).
[56] S. Sorella, Phys. Rev. B **71**, 241103 (2005).
[57] S. Sorella, Phys. Rev. B **64**, 024512 (2001).
[58] F. Aryasetiawan, M. Imada, A. Georges, G. Kotliar, S. Biermann, and A. I. Lichtenstein, Phys. Rev. B **70**, 195104 (2004).
[59] N. Lanatà, P. Barone, and M. Fabrizio, Phys. Rev. B **78**, 155127 (2008).
[60] R. Fletcher, *Practical Methods of Optimization* (Wiley & Sons, New York, 1987).
[61] D. M. Ceperley and B. J. Alder, Phys. Rev. Lett. **45**, 566 (1980).
[62] H. J. Monkhorst and J. D. Pack, Phys. Rev. B **13**, 5188 (1976).
[63] R. D. Cowan, *Theory of Atomic Structure and Spectra* (University of California Press, Oakland, 1981).
[64] W. Setyawan and S. Curtarolo, Comput. Mater. Sci. **49**, 299 (2010).
[65] E. G. Moroni, G. Kresse, J. Hafner, and J. Furthmüller, Phys. Rev. B **56**, 15629 (1997).
[66] C. Zener, Phys. Rev. **82**, 403 (1951).
[67] P. W. Anderson and H. Hasegawa, Phys. Rev. **100**, 675 (1955).
[68] J. M. D. Coey, M. Viret, and S. von Molnár, Adv. Phys. **48**, 167 (1999).
[69] E. C. Stoner, Proc. R. Soc. London, Ser. A **165**, 372 (1938).
[70] J. W. Lynn, Phys. Rev. B **11**, 2624 (1975).
[71] R. Joynt, J. Phys. F: Met. Phys. **14**, 2363 (1984).
[72] J. M. Leger, C. Loriers-Susse, and B. Vodar, Phys. Rev. B **6**, 4250 (1972).
[73] L. W. Shacklette, Phys. Rev. B **9**, 3789 (1974).
[74] M. Yousuf, P. C. Sahu, and K. G. Rajan, Phys. Rev. B **34**, 8086 (1986).
[75] M. E. Fisher and J. S. Langer, Phys. Rev. Lett. **20**, 665 (1968).
[76] S. Q. Wang, W. E. Evenson, and J. R. Schrieffer, Phys. Rev. Lett. **23**, 92 (1969).
[77] J. Sánchez-Barriga, J. Braun, J. Minár, I. Di Marco, A. Varykhalov, O. Rader, V. Boni, V. Bellini, F. Manghi, H. Ebert, M. I. Katsnelson, A. I. Lichtenstein, O. Eriksson, W. Eberhardt, H. A. Dürr, and J. Fink, Phys. Rev. B **85**, 205109 (2012).
[78] J. Schäfer, M. Hoinkis, E. Rotenberg, P. Blaha, and R. Claessen, Phys. Rev. B **72**, 155115 (2005).
[79] J. Sánchez-Barriga, J. Fink, V. Boni, I. Di Marco, J. Braun, J. Minár, A. Varykhalov, O. Rader, V. Bellini, F. Manghi, H. Ebert, M. I. Katsnelson, A. I. Lichtenstein, O. Eriksson, W. Eberhardt, and H. A. Dürr, Phys. Rev. Lett. **103**, 267203 (2009).
[80] M. Karolak, G. Ulm, T. Wehling, V. Mazurenko, A. Poteryaev, and A. Lichtenstein, J. Electron Spectrosc. Relat. Phenom. **181**, 11 (2010)
[81] W. Weber, J. Bünemann, and F. Gebhard, Lect. Notes Phys. **580**, 9 (2001).
[82] J. Bünemann, F. Gebhard, T. Ohm, S. Weiser, and W. Weber, in *Frontiers in Magnetic Materials*, edited by A. Narlikar (Springer, Berlin, 2005), pp. 117–151.
[83] J. Bünemann, F. Gebhard, T. Ohm, S. Weiser, and W. Weber, Phys. Rev. Lett. **101**, 236404 (2008).
[84] J. Hubbard, Phys. Rev. B **19**, 2626 (1979).
[85] T. Inui, Y. Tanabe, and Y. Onodera, *Group Theory and Its Applications in Physics* (Springer, New York, 1996).
[86] M. Tinkham, *Group Theory and Quantum Mechanics* (Dover, Mineola, NY, 1964).
[87] Z. Gimbutas and L. Greengard, J. Computat. Phys. **228**, 5621 (2009).